

Dephasing due to electromagnetic interactions in spatial qubits

Martine Schut^{1,2}, Herre Bosma¹, MengZhi Wu¹, Marko Toroš³, Sougato Bose⁴, and Anupam Mazumdar¹

¹*Van Swinderen Institute for Particle Physics and Gravity, University of Groningen, 9747 AG Groningen, the Netherlands*

²*Bernoulli Institute for Mathematics, Computer Science and Artificial Intelligence, University of Groningen, 9747 AG Groningen, the Netherlands*

³*School of Physics and Astronomy, University of Glasgow, Glasgow, G12 8QQ, United Kingdom*

⁴*Department of Physics and Astronomy, University College London, Gower Street, WC1E 6BT London, United Kingdom*



(Received 26 January 2024; revised 17 June 2024; accepted 9 July 2024; published 8 August 2024)

Matter-wave interferometers with microparticles will enable the next generation of quantum sensors to probe minute quantum phase information. Therefore, estimating the loss of coherence and the degree of entanglement degradation for such interferometers is essential. In this paper, we provide a noise analysis in frequency-space focusing on electromagnetic sources of dephasing. We assume that our matter-wave interferometer has a residual charge or dipole which can interact with a neighboring particle in the ambience. We investigate the dephasing due to the Coulomb, charge-induced dipole, charge-permanent dipole, and dipole-dipole interactions. All these interactions constitute electromagnetically driven dephasing channels that can affect single or multiple interferometers. As an example, we apply the obtained formulas to situations with two adjacent microparticles, which can provide insight for the noise analysis in the quantum gravity-induced entanglement of masses (QGEM) protocol and the C-NOT gate: we compute the dephasing due to a gas of environmental particles interacting via dipole-dipole and charge-charge couplings, respectively. To obtain simple analytical dephasing formulas, we employ uniform probability distributions for the impact parameter and for the angles characterizing the relative orientation with respect to the interferometer and a Gaussian distribution for the velocities of the environmental particles. In both cases, we show that the dephasing rate grows with the number density of particles present in the vacuum chamber, as expected.

DOI: [10.1103/PhysRevA.110.022412](https://doi.org/10.1103/PhysRevA.110.022412)

I. INTRODUCTION

One of the key features of quantum mechanics is the matter-wave duality exhibited in interferometry with massive systems [1]. Matter-wave interferometry has played a central role in many experimental breakthroughs in quantum mechanics [2–4], and also illustrates the idea of the spatial quantum superposition [5]. Matter-wave interferometry has been used to detect the Earth’s gravitationally induced phase in a series of seminal experiments with neutrons and atoms [6–10]. Moreover, it has been suggested as a tool for sensing gravitational waves [11], neutrinos [12], and as a probe for physics beyond the standard model [13].

When two or more interferometers can be placed adjacent to each other they can also test the quantum entanglement feature [14–16]. Recently, it has been suggested that matter-wave interferometry with microparticles will be sensitive enough to probe the quantum gravity-induced entanglement of masses (QGEM) [17,18], see also Ref. [19]. The entanglement between two adjacent matter-wave interferometers will be observed if gravity is a quantum-mechanical entity. In contrast, no entanglement will be generated if gravity is inherently classical as formalized by the local operations and classical communication (LOCC) theorem [17,20–22]. Such entangled pairs also provide the basis for a quantum computer as they form the CONTROLLED-NOT (CNOT) gate, or the Mølmer-Sørensen gate in the context of an ion trap [23]. One can go one step further and test the quantum light bending

interaction [24], the quantum version of the equivalence principle [25,26], test for massive graviton [27], nonlocal aspects of quantum gravity [28], and verify the quantum nature of gravity in the process of measurement [29].

Given so many applications on the horizon of the next generation of matter-wave interferometers, it is essential to understand various causes of decoherence and dephasing. Large spatial quantum superpositions [30–40] have to remain coherent for the duration of the experiment to extract their delicate experimental signature [41–50]. Here we focus on electromagnetic sources of dephasing induced by ambient particles located in the vicinity of the interferometric setup.

First, we consider a single matter-wave interferometer. We investigate the acceleration noise caused by a single particle passing by the interferometer and estimate how it will dephase the matter-wave interferometer via electromagnetic interactions. Then, we consider if two such entangled interferometers were kept adjacent; the source of acceleration noise will also contribute to entanglement degradation. If the matter-wave interferometer consists of a neutral microparticle, the dominant contribution to the acceleration results from its dipole (either permanent or induced). If the microparticle possesses any residual charge, such a charged interferometer can interact with an ambient charged particle or an ambient neutral particle possessing a dipole (either permanent or induced). The common aspect of all these interactions is that the moving particle will always create a slight jitter in the paths of the interferometer introducing noise

and thus dephasing. We analyze these cases systematically and quantify each scenario's resulting loss of coherence.

To analyze the electromagnetic acceleration noise and dephasing we employ the frequency space techniques, which are commonly used to investigate Newtonian noise [51]. The reason is that the Coulomb and Newtonian interactions are long range and provide a $1/r$ potential, resulting in an infinite total cross-section unless a cutoff for small scattering angles is applied [52]. Since the computations of the decoherence rate based on the scattering theory generally depend on the total cross section, see Refs. [47,53], at least for long-range interactions, we have to use an alternative methodology. In this paper, we adapt the methodology based on the Feynman path-integral approach following Storey and Cohen-Tannoudji [54], which we have previously used to investigate noninertial and gravity gradient noise [55,56], to the case of electromagnetic interactions.

We begin the paper with a generic discussion on relative acceleration noise (Sec. II), which we apply to electromagnetic noise sources. We discuss the case of a charged and a neutral interferometer (Sec. III). First, the interaction between the charged interferometer and an external charge (Coulomb interaction), and the interaction between the charged interferometer and an induced or permanent external dipole (charge-dipole interaction) (Sec. IV). Second, we analyze the neutral interferometer particle with a permanent or induced dipole that interacts with an external charge (dipole-charge interaction) or with an external dipole (dipole-dipole interaction) (Sec. V).

II. RELATIVE ACCELERATION NOISE

This section introduces the main tools for describing relative acceleration noise (RAN) in frequency space. We then discuss how to compute the resulting dephasing from the associated phase noise. In a nutshell, any movement of charges or dipoles in the vicinity of the matter-wave interferometer will cause a tiny jitter or acceleration noise, which we denote here by $a_{\text{noise,EM}}$, which will induce phase fluctuations and hence dephasing. The subscript EM denotes electromagnetic-type external interactions.

We assume that the spatial superposition state can be created via the Stern-Gerlach (SG) setup, as it happens in spin-embedded systems with a nitrogen vacancy (NV). We can envisage a spin-magnetic-field interaction responsible for creating the superposition, e.g., using an SG apparatus, similar to what has been applied to the atomic case [33,35,36,57] and charged case [58]. The other possibility will be to create a spatial superposition in an ion trap [59–61]. In either case, the matter-wave interferometer will be considered a spatial qubit, where interactions with an environment can induce a relative phase between the interferometer's two arms (or the spatial superposition states of the spatial qubit).

A. General noise analysis

The difference in the phase picked up between the two arms of an interferometer is determined by the difference in the actions of the two trajectories. Taking the superposition to be along one dimension, e.g., in the \hat{x} direction, without any

loss of generality, it follows that the difference in phase-shift is given by [54]

$$\begin{aligned} \delta\phi &= \phi_R - \phi_L \\ &= \frac{1}{\hbar} \int_{t_i}^{t_f} L_R[x_R, \dot{x}_R] - L_L[x_L, \dot{x}_L] dt, \end{aligned} \quad (1)$$

where ϕ_i and L_i are the phases and the Lagrangians for $i = L, R$, the left and the right arm of the superposition, respectively. Here, we consider a single interferometer; we consider the case of adjacent interferometers later. The bounds of the integral are equal to the time of splitting and recombination of the two trajectories to complete a one-loop interferometer. The time when the interferometer is in a spatial superposition is given by $\tau = t_f - t_i$, where f, i stands for the interferometer's final and initial time.

Here, we consider the nonrelativistic regime of a free-falling test mass split into the superposition by an acceleration, λ_j , in the \hat{x} direction.¹ The Lagrangian of the two arms of the interferometer (with mass m) can be expressed as

$$L_j = \frac{1}{2}mv_j^2 - m\lambda_j(t)x_j - ma_{\text{noise,EM}}(t)x_j. \quad (2)$$

We wish to close the trajectories (recombine the spatial qubit into a spin qubit) so that the wave functions of both trajectories nearly overlap. If they do not, there will be a substantial loss of visibility. If the spread of the wave packets is σ then one would require $|X_L(t_f) - X_R(t_f)| \ll \sigma$ to achieve the required visibility [63–65].

The noise we consider in the trajectories can be modeled by the fluctuations in the phase, given by the last term in Eq. (2). We assume that $a_{\text{noise,EM}}$ is independent of the force responsible for creating the superposition but that it is time-dependent during $\tau = t_f - t_i$. Hence, the fluctuation in the phase shift at the leading order due to the EM interaction will be given by

$$\delta\phi = \frac{m}{\hbar} \int_{t_i}^{t_f} a_{\text{noise,EM}}(t)(x_R - x_L) dt, \quad (3)$$

here $\delta\phi(t)$ will be treated as a statistical quantity. The measurable noise in any experiment is the statistical average of any stochastic entity, which we denote by $\mathbb{E}[\cdot]$. The averaging can be obtained over time using a single realization of the noise for a time-varying ergodic noise. For example, the average of a time-varying stochastic quantity $\delta\phi(t)$ can be expressed as

$$\mathbb{E}[\delta\phi] = \frac{1}{T} \int_0^T \delta\phi(t) dt, \quad (4)$$

where T is much larger than any timescale characterizing the noise. For simplicity of the analysis, we assume that the interferometric timescale is much shorter than the timescale T , i.e., $T \gg \tau$, where τ denotes the experimental time, $\tau = t_f - t_i$. Furthermore, we take T as the total time of the experiment (comprising repeated runs of the experimental sequence,

¹The acceleration of the two superposition states is due to the SG setup in the context of NV centered microparticles [17,34,62]. In the case of ions, the force exerted to create the superposition will be due to the photon kicks [59,60]. We can also envisage creating quantum superposition for the charged microspheres with the help of SG setup, see Ref. [58].

where the statistic is gathered). For concreteness, we set $T = b/v$ such that in the total experimental time, we sufficiently capture the experimental signature of the external EM source on the experimental statistics following Ref. [51].

While the average of the noise can often be assumed to be zero, the autocorrelation of the acceleration noise measured at different times, $\mathbb{E}[a_{\text{noise, EM}}(t_1), a_{\text{noise, EM}}(t_2)]$, is often nonzero. It is related to the power spectral density (PSD) of the noise, denoted by $S_{aa}(\omega)$. The definition of the PSD of the noise $a_{\text{noise, EM}}$ is

$$S_{aa}(\omega) = \lim_{T \rightarrow \infty} \frac{|a_{\text{noise, EM}}(\omega)|^2}{T}, \quad (5)$$

where $a_{\text{noise, EM}}(\omega)$ is the Fourier transform of $a_{\text{noise, EM}}(t)$ on the time domain $[0, T]$. According to the Wiener-Khinchin theorem, the autocorrelation function of a random process is given by the PSD of that process [66,67]:

$$\mathbb{E}[a_{\text{noise, EM}}(t_1)a_{\text{noise, EM}}(t_2)] = \frac{1}{2\pi} \int_{\omega_{\min}}^{\infty} S_{aa}(\omega) e^{i\omega(t_1-t_2)} d\omega, \quad (6)$$

where the minimum frequency $\omega_{\min} = 2\pi/(t_f - t_i)$ is the frequency resolution in the experiment.²In particular, signals and noises are sampled as a discrete finite data series, so the frequency-domain analysis has to be based on the discrete Fourier transform, which has such a frequency resolution [68].

Using the relation in Eq. (6) and the difference in phase-shift form Eq. (3), the variance $\mathbb{E}[(\delta\phi)^2]$ can be written in the Fourier space by

$$\Gamma_n = \mathbb{E}[(\delta\phi)^2] = \frac{1}{2\pi} \left(\frac{m}{\hbar}\right)^2 \int_{\omega_{\min}}^{\infty} d\omega S_{aa}(\omega) F(\omega). \quad (9)$$

where Γ_n in Eq. (9) is the variance in the noise,³ which is an observable entity, and $F(\omega)$ is known as the transfer function [55,56]. As shown below, Γ_n will be useful to estimate the dephasing for the two spatial qubits, adding up to any other

²For a real-valued random process $X(t)$, the PSD is defined as

$$S_X(\omega) = \lim_{T \rightarrow \infty} \frac{1}{T} \int_{-\frac{T}{2}}^{\frac{T}{2}} \int_{-\frac{T}{2}}^{\frac{T}{2}} \mathbb{E}[X(t_1)X(t_2)] e^{-i\omega(t_1-t_2)} dt_2 dt_1. \quad (7)$$

Assuming that the PSD is stationary (i.e., its properties such as mean and covariance do not change over time) and using the Wiener-Khinchin theorem, we find from Eq. (7):

$$S_X(\omega) = \int_{-\infty}^{\infty} \mathbb{E}[X(t)X(t+\tau)] e^{-i\omega\tau} d\tau, \quad (8)$$

where $\tau = t_2 - t_1$, and the result does not depend on the chosen value of t (e.g., we can set $t = 0$). Taking the Fourier transform gives Eq. (6).

³Although the term *noise* often signifies *unknown dynamics*, here we use it more loosely when referring to *unwanted interactions* with environmental particles which we cannot measure directly. The discussion is thus far generic and could span a number of different models of the environment. In later sections we assume specific probability distributions characterizing the environmental particles (i.e., a dilute gas of particles), and then compute the resulting dephasing after averaging over the distributions.

sources of decoherence caused by the external or internal degrees of freedom. Note that the Γ_n is a dimensionless entity.

The transfer function is equal to the absolute value squared of the Fourier transform of the difference in the trajectories:

$$F(\omega) = \left| \int_{t_i}^{t_f} dt (x_L - x_R) e^{i\omega t} \right|^2 = \left| -\frac{1}{\omega^2} \int_{t_i}^{t_f} \frac{d^2}{dt^2} (x_L - x_R) e^{i\omega t} dt \right|^2. \quad (10)$$

In the second line, we find the dependency on the acceleration, d^2x/dt^2 , which, as we will see, can be related to particle equations of motion, and follows from integration by parts and the equality of both the position and velocity at the path's endpoints from the first line.

The dephasing formula in Eq. (9) is still generic and applies to an arbitrary acceleration noise PSD $S_{aa}(\omega)$ and transfer function $F(\omega)$. In the next sections, we apply it to investigate specific cases of electromagnetic interactions, where the environment is made of gas particles characterized by probability distributions for the impact factor, velocities, and the relative angles with respect to the interferometer. The acceleration noise $S_{aa}(\omega)$ could be either obtained from independent measurements characterizing the environment of the experiment or by developing a microscopic modeling of the environment. To obtain simple formulas we consider a simple microscopic model of a dilute gas, where the particles move on straight lines, and the interaction among the environmental particles is neglected. The transfer function $F(\omega)$ is on the other hand determined by the interferometer and the type of interaction. In the next section we specify the form of $F(\omega)$ by assuming an idealized Stern-Gerlach interferometer.

B. Example of Stern-Gerlach interferometer

The dephasing in Eq. (9) is dependent on the specific trajectory of the two arms of the matter-wave interferometer [via the transfer function $F(\omega)$]. Here, we assume an SG-type interferometer that is often proposed in the context of entanglement-based quantum-gravity experiments, see Refs. [17,21,37–39,69].

We specify the trajectory of two arms of the interferometer; see Fig. 1. Here, we assume a symmetric path for the interferometer as a prototype model. We consider a simplistic scenario, assuming that the acceleration of the spin state j , denoted λ_j , is proportional to the gradient of the magnetic field, given by

$$\lambda_j = s_j \frac{g\mu_B}{m} |\nabla B|, \quad (11)$$

where s_j is the spin of the state, g is the Landé g factor of the electron ($g = 2$), $\mu_B = 9 \times 10^{-24} \text{ JT}^{-1}$ is the Bohr-magneton, m is the mass of the test-mass and $|\nabla B|$ is the magnitude of the gradient of the magnetic field. To create the path in Fig. 1, one controls the spin so that the acceleration of the right arms is positive from $[0, t_a]$ and $[3t_a + t_e, 4t_a + t_e]$ and negative from $[t_a, 2t_a]$ and $[2t_a + t_e, 3t_a + t_e]$, while it is zero for the time range $[2t_a, 2t_a + t_e]$. For the left arm, the spin and acceleration will be equal in magnitude but in the

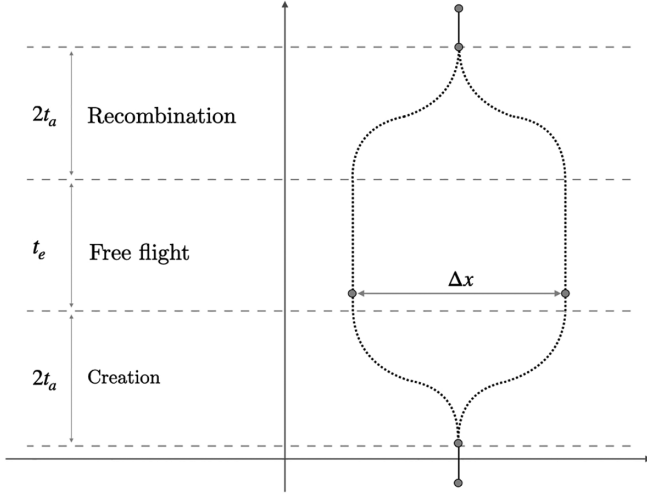


FIG. 1. Schematic illustration of the paths of the arms of the interferometer (adapted from Refs. [55,56]). Based on this figure, the transfer function in Eq. (12) can be calculated. For the left arm, the acceleration is in the negative direction from $[0, t_a]$ and $[3t_a + t_e, 4t_a + t_e]$, in the positive direction from $[t_a, 2t_a]$ and $[2t_a + t_e, 3t_a + t_e]$, while it is zero for the time range $[2t_a, 2t_a + t_e]$. Meanwhile, the acceleration is the opposite for the right arm.

opposite direction. We also assume $x_j(0) = 0$ and $\dot{x}_j(0) = 0$ for solving the equations of the motion for the trajectory, given by $\ddot{x}_j(t) = \lambda_j(t)$. Microparticles can be electrically charged by ultraviolet irradiation [70]. For a small number of charges n , the Lorentz force acting on the microparticle $\approx nevB/m$ (with e being the unit of electric charge) is negligible due to its large mass m , see Ref. [58]. With the help of the equations of motion, the transfer function corresponding to the trajectory illustrated in Fig. 1 can be computed:

$$F(\omega) = \frac{1}{\omega^2} \left| \int_{t_i}^{t_f} (\lambda_L - \lambda_R) e^{i\omega t} dt \right|^2 = \left| \frac{2}{\omega^2} \int_{t_i}^{t_f} \lambda_s e^{i\omega t} dt \right|^2 = \frac{32\lambda_s^2}{\omega^6} \sin^4\left(\frac{t_a\omega}{2}\right) \sin^2\left[\frac{\omega}{2}(2t_a + t_e)\right]. \quad (12)$$

Since how the superposition is created is immaterial, for the calculation of the transfer function, it is convenient to define the transfer function in terms of the maximal superposition size created after two acceleration times, $\Delta x = \lambda t_a^2$:

$$F(\omega) = \frac{32(\Delta x)^2}{\omega^6 t_a^4} \sin^4\left(\frac{t_a\omega}{2}\right) \sin^2\left[\frac{\omega}{2}(2t_a + t_e)\right]. \quad (13)$$

By finding the PSD, S_{aa} , due to different types of interaction and combining it with the specifics of the trajectory encoded in the transfer function in Eq. (13), we can find the noise via Eq. (9).

III. ELECTROMAGNETIC-INDUCED ACCELERATION NOISE

In this section, we investigate the situation of external particles interacting electromagnetically with our interferometer, causing spurious accelerations. We envisage a situation of a rarefied gas, where the external particles can be considered

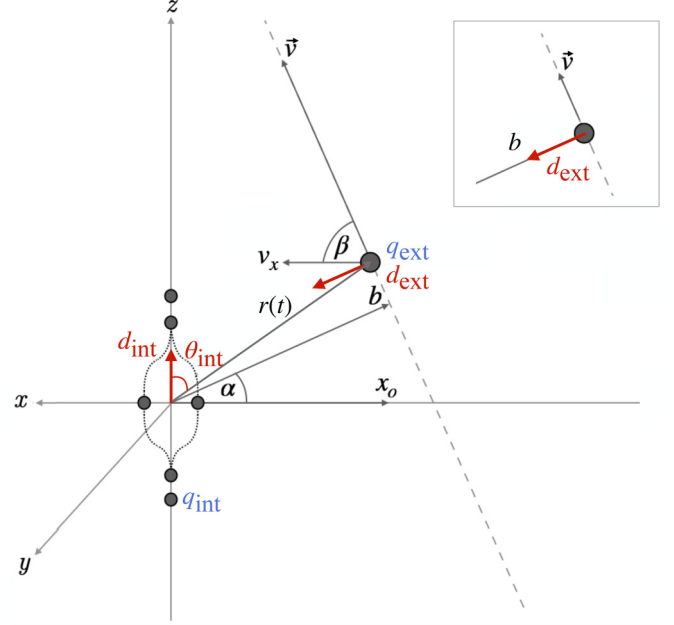


FIG. 2. Illustration of the interferometer and the external particle (i.e., the source of dephasing). The position of the closest approach is (x_0, y_0, z_0) corresponding to the impact parameter b (the center-of-mass of the interferometer is used for the definition since we assume $\Delta x \ll b$). The magnitude of the position vector is given by $|r| = [b^2 + (vt)^2]^{1/2}$, where the velocity is $v = |v| = (v_x, v_y, v_z)$. The projection angles are defined by $\cos(\alpha) = x_0/b$ and $\cos(\beta) = v_x/v$. The red arrows denote the dipole moments.

as independent sources of disturbance moving at constant velocity. More refined models of the gaseous environment (e.g., which would include interactions among environmental particles, etc.) could be obtained by refining the model of $S_{aa}(\omega)$, which will be presented below.

We assume that the individual external particle is moving with a constant velocity v and with an impact parameter b for the matter-wave interferometer (see Fig. 2). The position of the external particle concerning the matter-wave interferometer can be conveniently described by the vector $r(t)$ from the interferometer center of mass to the external particle, with length:

$$r(t) = \sqrt{b^2 + (vt)^2}. \quad (14)$$

The x component of this vector, from the properties of the setup (see Fig. 2), is $r_x(t) = x_0 + v_x t$. The unit vector in the x direction is denoted by \hat{r}_x , and x_0 and v_x are defined to be the x components of the impact parameter b and velocity v , respectively. We can thus introduce the projection angles:

$$\cos(\alpha) = x_0/b, \quad \cos(\beta) = v_x/v. \quad (15)$$

The acceleration PSD in the considered situation is thus parametrized by four parameters:

$$S_{aa}(\omega) \equiv S_{aa}(b, v, \alpha, \beta; \omega). \quad (16)$$

As these parameters are unknown, we can treat them as random variables characterized by their respective probability distributions. The averaged acceleration noise PSD is given

by

$$\begin{aligned} \bar{S}_{aa}(\omega) = N \int db \int dv \int d\alpha \int d\beta p_b(b) p_v(v) \\ \times p_\alpha(\alpha) p_\beta(\beta) S_{aa}(b, v, \alpha, \beta; \omega), \end{aligned} \quad (17)$$

where N denotes the number of external particles in the experimental chamber, $p_b(b)$ is the distribution of the impact factors, $p_v(v)$ is the velocity distribution, and $p_\alpha(\alpha)$ and $p_\beta(\beta)$ are the distributions of the relative orientations. We suppose that the probability distributions are given by⁴

$$p_b(b) = \frac{3b^2}{L^3}, \quad b \in [R, L], \quad (18)$$

$$p_v(v) = \left[\frac{m_{\text{gas}}}{2\pi k_B T_{\text{gas}}} \right]^3 4\pi v^2 e^{-\frac{m_{\text{gas}} v^2}{2k_B T_{\text{gas}}}}, \quad v \in [0, \infty], \quad (19)$$

$$p_\alpha(\alpha) = \frac{1}{2\pi}, \quad \alpha \in [0, 2\pi], \quad (20)$$

$$p_\beta(\beta) = \frac{1}{2\pi}, \quad \beta \in [0, 2\pi], \quad (21)$$

where L denotes the size of the experimental chamber, R is the radius of the test mass, m_{gas} is the mass of the gas particle, and T_{gas} is the temperature of the gas. The number density of particles is thus $n_v = N/V$. As the gas particles are assumed noninteracting in our modeling (i.e., rarefied gas), we have assumed the Maxwell–Boltzmann distribution for the velocities. As we discuss in the following sections, the Maxwell–Boltzmann distribution can be at low temperatures approximated by a narrow Gaussian distribution or in first instance by a Dirac delta distribution. Using the ideal-gas law we can then equivalently also investigate the behavior of the dephasing as a function of the pressure $p = nk_B T_{\text{gas}}$. The corresponding averaged dephasing factor $\bar{\Gamma}_n$ can be computed using Eq. (9) by formally replacing S_{aa} with $\bar{S}_{aa}(\omega)$.

The moving external particles can cause a random acceleration noise on the interferometer due to the EM interactions, contributing to a phase fluctuation of the interferometer. In the following, we first explore the behavior of the nonaveraged acceleration PSD $S_{aa}(b, v, \alpha, \beta; \omega)$ and of the resulting dephasing factor Γ_n defined in Eq. (9). Such an analysis provides an indication of the allowed parameter space of b, v, α, β for the dephasing to remain contained (see Secs. IV–VI). We then compute the averaged acceleration PSD $\bar{S}_{aa}(\omega)$ and the corresponding averaged dephasing $\bar{\Gamma}_n$ using the probability distributions in Eqs. (18)–(21) for two applications (Sec. VII).

We suppose the microparticle and the moving particle can be modeled as either point charges or dipoles and consider two cases for the interactions.

⁴The distribution of the velocity is taken to be Maxwell–Boltzmann. The distributions for the projection angles and the impact parameter are uniform. The integrations over the projection angles are divided by the total angle 2π to get an average angle. The distribution for the impact parameter is taken to be uniform in Cartesian coordinates and rewritten in terms of spherical coordinates.

A. Charged interferometer

If the interferometer is charged, the microcrystal has an overall charge. Then, there can be two EM interactions between the charged interferometer and the external particle:

(1) A charge-charge interaction between the external charge, q_{ext} , and the charge of the interferometer, denoted here by q_{int} . The Coulomb potential gives this interaction:

$$V_{\text{cc}}(r) = \frac{1}{4\pi\epsilon_0} \frac{q_{\text{int}} q_{\text{ext}}}{r}, \quad (22)$$

where both systems are considered as point charges.

(2) A charge-dipole interaction between the charge of the interferometer, q_{int} , and the dipole of the external particle, \mathbf{d}_{ext} . This interaction is given by the potential, see Refs. [71,72],

$$V_{\text{cd}}(r) = \frac{q_{\text{int}}}{4\pi\epsilon_0} \frac{\mathbf{d}_{\text{ext}} \cdot \hat{\mathbf{r}}}{r^2}. \quad (23)$$

The external dipole can be either induced or permanent.

B. Neutral interferometer

If the interferometer is neutral, there can be two types of EM interactions between the interferometer and the external particle.

(1) A dipole-charge interaction between the dipole of the interferometer, \mathbf{d}_{int} (which can be either permanent or induced by the EM field of the external particle), and the charge of the external particle, q_{ext} . This interaction is given by the potential [71]

$$V_{\text{dc}}(r) = -\frac{q_{\text{ext}}}{4\pi\epsilon_0} \frac{\mathbf{d}_{\text{int}} \cdot \hat{\mathbf{r}}}{r^2}, \quad (24)$$

where the external particle is assumed to be a point charge.

(2) A dipole-dipole interaction, where the dipole of the interferometer, \mathbf{d}_{int} , and the dipole of the external particle, \mathbf{d}_{ext} , are assumed to be permanent. This interaction is given by the potential [71,72]

$$V_{\text{dd}}(r) = \frac{1}{4\pi\epsilon_0} \left[\frac{\mathbf{d}_{\text{int}} \cdot \mathbf{d}_{\text{ext}}}{r^3} - \frac{3(\mathbf{d}_{\text{int}} \cdot \hat{\mathbf{r}})(\mathbf{d}_{\text{ext}} \cdot \hat{\mathbf{r}})}{r^3} \right], \quad (25)$$

where $\hat{\mathbf{r}}$ is the unit vector pointing in the direction from the interferometer center of mass to the external particle center of mass.

C. Accelerations due to charged and neutral interactions

These interaction potentials will cause a random noise on the interferometer $a_{\text{noise, EM}}$, which will contribute a phase fluctuation that can be detectable by sensing it if we were to use the matter-wave interferometer as a quantum sensor, or this acceleration noise will lead to dephasing the experimental outcome in a QGEM-type experiment for instance. We now give a brief outline of all the accelerations. For each of the interactions discussed above, Eqs. (22)–(25), the corresponding acceleration is found via $\mathbf{F} = m\mathbf{a}$, with $\mathbf{F} = -\partial V/\partial \mathbf{r}$, where m is the mass of the interferometer.

$$\mathbf{a}_{\text{cc}} = \frac{q_{\text{int}} q_{\text{ext}}}{4\pi m \epsilon_0} \frac{\hat{\mathbf{r}}(t)}{r^2(t)}, \quad (26)$$

$$\mathbf{a}_{\text{cd}} = \frac{q_{\text{int}}}{2\pi m \epsilon_0} \frac{\mathbf{d}_{\text{ext}} \cdot \hat{\mathbf{r}}(t)}{r^3(t)} \hat{\mathbf{r}}(t), \quad (27)$$

$$a_{dc} = \frac{q_{\text{ext}}}{2\pi m \epsilon_0} \frac{\mathbf{d}_{\text{int}} \cdot \hat{\mathbf{r}}(t)}{r^3(t)} \hat{\mathbf{r}}(t), \quad (28)$$

$$a_{dd} = \frac{3\hat{\mathbf{r}}}{4\pi \epsilon_0 m} \left[\frac{\mathbf{d}_{\text{ext}} \cdot \mathbf{d}_{\text{int}}}{r^4(t)} - 3 \frac{(\mathbf{d}_{\text{ext}} \cdot \hat{\mathbf{r}})(\mathbf{d}_{\text{int}} \cdot \hat{\mathbf{r}})}{r^4(t)} \right]. \quad (29)$$

The vector $\hat{\mathbf{r}}$ is time-dependent and given by $\hat{\mathbf{r}}(t) = \mathbf{r}(t)/r(t)$, with $r(t) = |\mathbf{r}(t)|$ [as defined in Eq. (14)]. The dipole can be either permanent or induced, which we distinguish with the notation $\mathbf{d}(i)$ and $\mathbf{d}(p)$, respectively.

Since the interferometer is created in one dimension, e.g., \hat{x} direction in our case, the only relevant acceleration is in the \hat{x} direction, and we are specifically interested in $a_x(t)$. The acceleration is found separately now for every interaction in Eqs. (22)–(25), and some assumptions are made on the orientation of the dipole vectors for simplification and to estimate the upper bound on the dephasing.

The mean value of the noise can be assumed to be zero, e.g.,

$$\mathbb{E}[a_{\text{noise, EM}}] = \mathbb{E}[\delta\phi] = 0. \quad (30)$$

This is because the zero point, or the baseline of the phase, can be calibrated using an auxiliary experiment, so the contribution of the mean value of every noise will be considered in the offset of the baseline in our current analysis. Therefore, we here focus on finding the autocorrelation of the acceleration noise at different times, $\mathbb{E}[a_{\text{noise, EM}}(t_1), a_{\text{noise, EM}}(t_2)]$, see Eq. (6). Taking the Fourier transform to find $a_x(\omega)$ on the time domain $[0, T]$, we can use Eq. (5) to find the noise PSD $S(\omega) = |a_x(\omega)|^2/T$. Combining the noise PSD with the transfer function gives the dephasing using Eq. (9). The results for the noise are given in Secs. IV and V, and the detailed calculations are presented in Appendix A.

IV. DEPHASING OF A CHARGED INTERFEROMETER

If there is some charge on the interferometric particle, then charge-charge interactions and charge-external dipole interactions will generate acceleration noise in the system. We consider the charge-charge interaction and the charge-dipole interaction between the interferometer and the external particle, where we investigate separately the dipole of the external particle to be permanent or induced.⁵

A. Dephasing due to internal charge and external charge interaction

First of all, we assume the simplest case of a charged matter-wave interferometer: the matter-wave interferometer has a charge q_{int} , which is interacting with ambient charge q_{ext} that is moving with a constant velocity and has the closest approach b from the interferometer's center of mass. The

⁵These interactions depend on the relative sign of the charges and dipoles (whether they are attractive or repulsive). In this section, we do not specify the relative sign because we are interested in finding the dephasing, and we note that this is proportional to the acceleration *squared*. The dephasing is therefore independent of the sign of the interaction potential.

acceleration due to the charge-charge interaction in the \hat{x} direction is given by

$$a_x^{\text{cc}}(t) = \frac{q_{\text{int}}q_{\text{ext}}}{4\pi \epsilon_0 m b^2} \frac{\cos(\alpha) + (vt/b)\cos(\beta)}{[1 + (vt/b)^2]^{3/2}}. \quad (31)$$

Finding S_{aa} from $a_x(\omega)$ and putting it in Eq. (9) yields the dephasing

$$\Gamma_n^{\text{cc}} = \frac{q_{\text{int}}^2 q_{\text{ext}}^2 (\Delta x)^2}{\pi^3 \hbar^2 \epsilon_0^2 T v^4 t_a^4} \int_{\omega_{\text{min}}}^{\infty} \omega^{-4} \sin^2 \left[\frac{\omega}{2} (2t_a + t_e) \right] \\ \times \sin^4 \left(\frac{t_a \omega}{2} \right) \left[\cos^2(\alpha) K_1^2 \left(\frac{b\omega}{v} \right) \right. \\ \left. + \cos^2(\beta) K_0^2 \left(\frac{b\omega}{v} \right) \right] d\omega. \quad (32)$$

with K_ν is the modified Bessel function (see Appendix A). The dephasing depends on the charges q_{int} and q_{ext} , the size of the spatial superposition and the time during which it is created, the impact parameter, and the velocity of the external particle. Furthermore, the time T , the time over which the phase fluctuations are averaged, and the minimum frequency ω_{min} are determined by the experimental setup, impact parameter b , and the velocity v of the external particle. The integral in Eq. (32) is solved numerically, and the resulting dephasing is plotted in Sec. VI [Fig. 3(a)] for a specific interferometer scheme.

B. Dephasing due to internal charge and external dipole interaction

This section will consider a charged interferometer particle interacting with an external dipole. The dipole could arise from any ambient gas particle inside the vacuum chamber. We only consider the acceleration noise due to one such external particle. The water vapor left in the vacuum chamber consists of the water molecules that carry a permanent dipole moment. Left-over air molecules in the vacuum chamber, such as dinitrogen, carbon dioxide, argon and dioxygen, are polarizable and could thus have an induced dipole moment from the charge of the interferometer. The acceleration due to the charge-dipole interaction is given in Eq. (27), and the acceleration depends on whether the dipole is induced or permanent.

1. Permanent external dipole

Suppose the external particle has a permanent dipole, such as in the case of water vapor. In that case, the dipole moment magnitude can be taken to be the experimentally determined value, e.g., $\mathbf{d}_{\text{ext}}^{(p)} = 6.19 \times 10^{-30}$ Cm in the case of water vapor (the superscript p standing for permanent) [73]. Taking the worst-case scenario, we assume that, at the point of closest approach b , the dipole vector of the external particle is aligned with the vector $\mathbf{r}(t)$.

Assuming that the particle moves very slowly, we maximize the acceleration by taking the dipole vector and the vector $\mathbf{r}(t)$ to align during the experimental time $\tau = t_f - t_i$. The acceleration in the x direction can be found to be

$$a_x^{\text{cd}(p)}(t) = \frac{q|\mathbf{d}_{\text{ext}}|}{2\pi m b^3 \epsilon_0} \frac{\cos(\alpha) + (vt/b)\cos(\beta)}{[1 + (vt/b)^2]^2}. \quad (33)$$

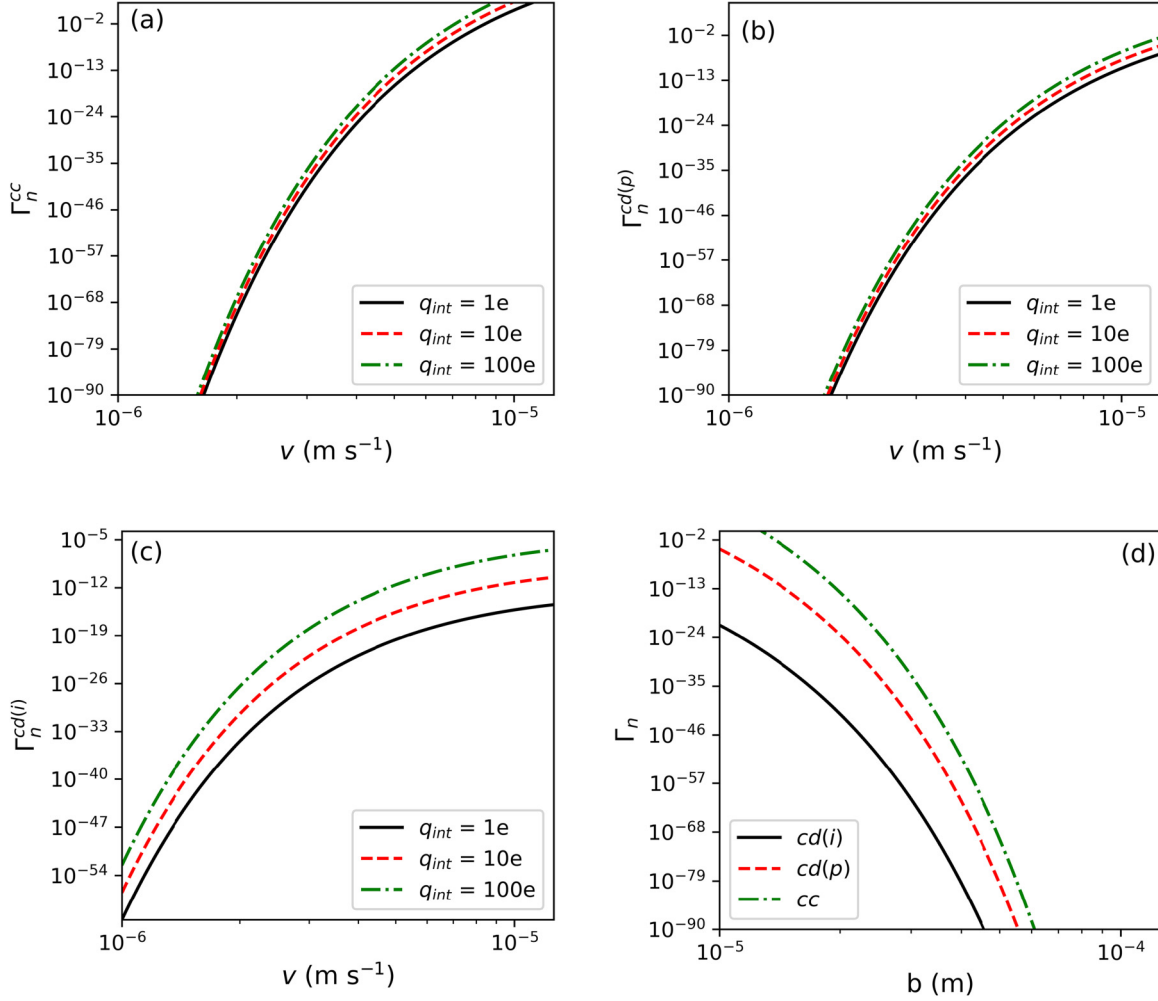


FIG. 3. Dephasing as a function of the velocity of the external particle due to (a) the charge-charge interaction (cc), (b) the charge-permanent dipole interaction [cd(p)] and (c) the charge-induced dipole interaction [cd(i)], for a different number of interferometer charges. The expressions summarized in Table I are plotted, where the integral is solved numerically. Projection angles $\alpha = \beta = 0$ and $T = b/v$. We have taken $\Delta x = 20 \mu\text{m}$ in all the plots. In panel (a) $b = 100 \mu\text{m}$ and the external charge is that of an electron, in Fig. (b) $b = 100 \mu\text{m}$ and the external dipole moment d_{ext} is that of a water molecule, in Fig. (c) $b = 30 \mu\text{m}$ and the external particle's polarizability is that of the dinitrogen. Panel (d) shows the different dephasing for a charged interferometer as a function of the impact parameter, for $v = 1 \mu\text{m s}^{-1}$, $q_{int} = e$ and the interaction-specific parameters discussed above. This plot (d) shows that the interferometer could detect a $q_{ext} = e$ charged particle moving with a velocity $v = 1 \mu\text{m s}^{-1}$ in the vicinity of $10 \mu\text{m}$. The Coulomb interaction provides the largest dephasing compared with the charge dipole interactions. In all the plots we have ensured $T \sim b/v > \tau \approx 3 \text{ s}$.

Its Fourier transforms and the resulting PSD of the noise are given in Appendix A. The dephasing is then given by Eq. (9), and the full integral will be

$$\begin{aligned} \Gamma_n^{cd(p)} &= \frac{q^2 |\mathbf{d}_{ext}|^2 (\Delta x)^2}{2\pi^2 \hbar^2 \epsilon_0^2 T v^5 b t_a^4} \int_{\omega_{min}}^{\infty} \omega^{-3} \sin^2 \left[\frac{\omega}{2} (2t_a + t_e) \right] \\ &\times \sin^4 \left(\frac{t_a \omega}{2} \right) \left[\cos^2(\alpha) K_{3/2}^2 \left(\frac{b\omega}{v} \right) \right. \\ &\left. + \cos^2(\beta) K_{1/2}^2 \left(\frac{b\omega}{v} \right) \right] d\omega, \end{aligned} \quad (34)$$

where K_ν is the modified Bessel function (see Appendix A). The results of the integration with the parameters of a specific interferometer setup are given in Sec. VI [Fig. 3(b)].

2. Induced external dipole

Left-over air molecules in the vacuum chamber have a polarizability of $\alpha_{pol} \approx 10^{-40} \text{ A}^2 \text{ s}^4 \text{ kg}$.⁶ If the dipole moment in the external particle with polarizability is induced due to the electric field \mathbf{E} from the charged interferometer, then the result is slightly different. The induced dipole by a charge q_{int} is given by

$$\mathbf{d}_{ext}^{(i)} = \alpha_{pol} \mathbf{E} = \alpha_{pol} \frac{q_{int}}{4\pi \epsilon_0 r^2} \hat{\mathbf{r}}, \quad (35)$$

⁶Generally this polarizability is expressed in CGS units, $\alpha'_{pol} = 1.5\text{--}2.5 \text{ \AA}^3$ [74,75], where $1 \text{ \AA}^3 = 10^{-24} \text{ cm}^3$. Which is related to the polarizability in SI units, $\text{A}^2 \text{ s}^4 \text{ kg}^{-1}$, via $\alpha_{pol} = 4\pi \epsilon_0 \alpha'_{pol}$. The particle polarizability is related to the average electric susceptibility of a medium, ϵ , via the Clausius–Mossotti relation, see Eq. (39).

where the superscript (i) stands for induced. The acceleration in the \hat{x} direction thus becomes

$$\begin{aligned} a_x^{\text{cd(i)}}(t) &= \frac{q_{\text{int}}^2 \alpha_{\text{pol}} \cos(\alpha) + (vt/b) \cos(\beta)}{8\pi^2 mb^5 \epsilon_0^2} \frac{1}{[1 + (vt/b)^2]^2} \frac{1}{r^2(t)}, \\ &= \frac{q_{\text{int}}^2 \alpha_{\text{pol}} \cos(\alpha) + (vt/b) \cos(\beta)}{8\pi^2 mb^5 \epsilon_0^2} \frac{1}{[1 + (vt/b)^2]^3}. \end{aligned} \quad (36)$$

Appendix A presents the Fourier transform and PSD. The dephasing is then found to be

$$\begin{aligned} \Gamma_n^{\text{cd(i)}} &= \frac{q^4 \alpha_{\text{pol}}^2 (\Delta x)^2}{512\pi^4 \hbar^2 \epsilon_0^4 v^7 b^3 T t_a^4} \int_{\omega_{\text{min}}}^{\infty} d\omega \frac{1}{\omega} \sin^4\left(\frac{t_a \omega}{2}\right) \\ &\quad \times \sin^2\left[\frac{\omega}{2}(2t_a + t_e)\right] \left[\cos^2(\alpha) K_{5/2}^2\left(\frac{b\omega}{v}\right) \right. \\ &\quad \left. + \cos^2(\beta) K_{3/2}^2\left(\frac{b\omega}{v}\right) \right]. \end{aligned} \quad (37)$$

K_ν is the modified Bessel function (see Appendix A). Again, this expression can be solved numerically to obtain the dephasing. The results of the integration with the parameters of a specific interferometer setup are given in Sec. VI [Fig. 3(c)].

Equation (45) differs from the permanent dipole result in Eq. (42) since the induced dipole is assumed to be caused by the interferometer charge. As a result, Eq. (45) depends on the interferometer charge and the polarizability of the external particle, α_{pol} . The magnitude of the induced dipole is distance-dependent, resulting in a different v , b dependence of Eq. (45) compared with the permanent dipole dephasing result.

V. DEPHASING OF A NEUTRAL INTERFEROMETER

In this section, we assume that the microparticles in the interferometer have a dipole d_{int} (either permanent or induced) and that it is interacting with an external charged particle (of charge q_{ext}) or external dipole (d_{ext}). We consider separately the microcrystal's permanent and induced dipole moments in the presence of a charge.

Although the dephasing results obtained in this section are generic, we apply them to the QGEM experiment where neutral diamond-type crystals of mass $\approx 10^{-15}$ kg are considered. We briefly discuss the two different dipoles of the microparticle in this context.

(1) Permanent dipole: The microcrystal may have a permanent dipole due to the surface's impurities or volume. The dipole moment of silica-type material SiO_2 was experimentally measured in Ref. [76], which showed that the material exhibits no clear correlation between mass and dipole moment. That being said, the microparticle spheres of size 10, 15, and 20 μm had permanent dipoles varying from $\approx (1000\text{--}5000) e \mu\text{m}$, $\approx (200\text{--}8000) e \mu\text{m}$, and $\approx (8500 \pm 1500) e \mu\text{m}$ (for simplicity we use $e \mu\text{m}$ to express the dipole, with e a single electric charge such that $1 e \mu\text{m} \approx 1.6 \times 10^{-25}$ Cm). This shows at least an order of magnitude uncertainty in the permanent dipole magnitude. The study showed that this material's permanent dipole moments exhibit a volume scaling, leaving the question of whether the permanent dipole moment scales with the volume. For the test mass of radius $r = 0.5 \mu\text{m}$ (corresponding to $\approx 10^{-15}$ kg for a spherical diamond test mass), we take the dipole moment to be

$|d_{\text{int}}^{(p)}| \approx 0.1 e \mu\text{m}$, thus assuming a volume scaling, and using the experimental data in Ref. [76] as a benchmark.

(2) Induced dipole: The diamond-type crystal is a dielectric material, and the crystal has a polarizability α (in SI units $\text{A}^2 \text{s}^4 \text{kg}^{-1}$). In particular, in isotropic media, a local electric field will produce a local dipole in each atom of the crystal's lattice [72]:

$$d_{\text{int}}^{(i)} = N \alpha_{\text{pol}} E_{\text{loc}}. \quad (38)$$

The local polarizability (which we denote α_{pol}) of the atoms is related to the polarizability of the medium via the Clausius-Mossotti relation:

$$\frac{n \alpha_{\text{pol}}}{3 \epsilon_0} = \frac{\epsilon_r - 1}{\epsilon_r + 2}, \quad (39)$$

with n being the number density of atoms, $n = 3N/4\pi R^3$ for spherical masses (N is the number of atoms, R is the radius). As a result, the dipole for a spherical diamond crystal due to an external point charge q_{ext} is given by

$$d_{\text{int}}^{(i)} = \frac{\epsilon_r - 1}{\epsilon_r + 2} \frac{q_{\text{ext}} R^3}{r^2} \hat{r}, \quad (40)$$

with ϵ_r being the relative permittivity of the medium.

A. Dephasing due to internal dipole and charge interaction

We now consider the dephasing due to an internal dipole interacting with an external charge. The acceleration was given in Eq. (28), the x component of which depends on whether the dipole is permanent or induced.

1. Permanent dipole of a microparticle

Suppose the interferometer's microparticle has a permanent dipole moment, similar to that of silica-type material [76]. In that case, the dipole moment magnitude can be the experimentally determined value, e.g., $\approx e \mu\text{m}$ for microspheres, assuming a volume scaling as discussed previously. Furthermore, if we assume complete control of the interferometer particle, we can take the direction of the intrinsic dipole moment to be aligned with the \hat{z} axis. As detailed in Appendix A, in this scenario the component of the acceleration in the \hat{x} direction is

$$\begin{aligned} a_x^{\text{d(p)c}}(t) &= \frac{q_{\text{ext}} |d_{\text{int}}| \cos(\alpha) + (vt/b) \cos(\beta)}{2\pi mb^3 \epsilon_0} \frac{1}{[1 + (vt/b)^2]^{5/2}} \\ &\quad \times [\cos(\theta_0) + (vt/b) \cos(\gamma)], \end{aligned} \quad (41)$$

where γ is the angle between the velocity vector and the \hat{z} axis and θ_0 is the angle between the vector b and the \hat{z} axis (the angles γ , θ_0 are similar to the projection angles α , β , respectively, in Fig. 2 but γ , θ_0 are projection angles on the \hat{z} axis rather than on the \hat{x} axis; they are discussed in more detail in Appendix A).

The Fourier transform $a(\omega)$ gives an expression for the PSD, $S_{aa}(\omega)$, and from these expressions we find the dephasing parameter, see Appendix A. Taking the worst-case dephasing based on the angles α , β , γ , θ_0 (see Appendix B, where we optimize these angles to see the largest dephasing),

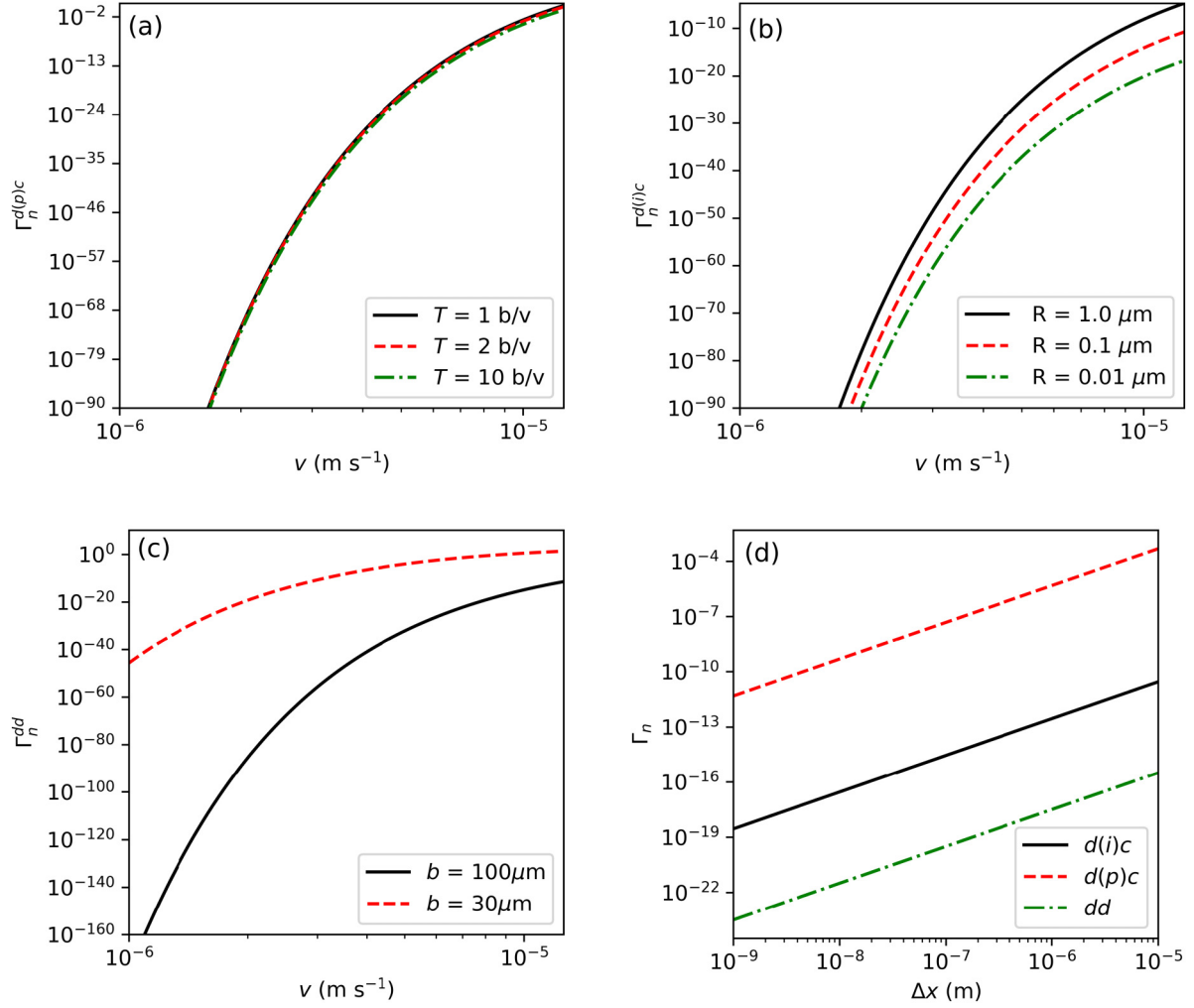


FIG. 4. Dephasing due to (a) the permanent dipole-charge interaction [d(p)c], (b) the induced dipole-charge interaction [d(i)c], and (c) the dipole-dipole interaction (dd) as a function of the velocity of the external particle. The expressions summarized in Table I are plotted, where the integral is solved numerically. With projection angles $\alpha = \beta = \gamma = \theta_0 = \pi/4$ for panel (a), $\alpha = \beta = 0$ for panel (b), and $\alpha = \theta_0 = \pi/4$, $\beta = 0$ for panel (c), see Appendix B. We take $\Delta x = 20 \mu\text{m}$ in all the cases. In panel (a) $b = 100 \mu\text{m}$, $d_{\text{int}} = 0.1 e \mu\text{m}$, and $q_{\text{ext}} = e$. Different lines for the noise timescale T are shown. There is not much noticeable difference in the dephasing rate due to different values of $T = b/v$. In panel (b) $b = 100 \mu\text{m}$, d_{int} is induced by the external charge $q_{\text{ext}} = e$ (with $\epsilon_r = 5.7$) and different lines for the interferometric particle's radius are plotted. In panel (c) $d_{\text{int}} = 0.1 e \mu\text{m}$ and the external particle is taken to be a water molecule, the dephasing is shown for different impact parameters. In panel (d), we summarize the dephasing from neutral microparticles interactions as a function of the superposition width Δx , for $v = 10 \mu\text{m s}^{-1}$, $b = 100 \mu\text{m}$, and the interaction-specific parameters discussed above for the charge and dipoles. The permanent dipole of a matter wave interferometer interacting with an external charge gives the largest dephasing here. We have ensured that $T = b/v > \tau \approx 3 \text{ s}$.

the dephasing is given as

$$\begin{aligned} \Gamma_n^{\text{d(p)c}} &= \frac{q_{\text{ext}}^2 |\mathbf{d}_{\text{int}}|^2 (\Delta x)^2}{9\pi^3 \epsilon_0^2 \hbar^2 v^6 T t_a^4} \int_{\omega_{\text{min}}}^{\infty} \frac{1}{\omega^2} \sin^4\left(\frac{t_a \omega}{2}\right) \\ &\times \left[K_2^2\left(\frac{b\omega}{v}\right) + \left(2 + \frac{b^2 \omega^2}{v^2}\right) K_1^2\left(\frac{b\omega}{v}\right) \right. \\ &\left. + K_0^2\left(\frac{b\omega}{v}\right) - 2 \frac{b\omega}{v} K_0\left(\frac{b\omega}{v}\right) K_1\left(\frac{b\omega}{v}\right) \right] \\ &\times \sin^2\left[\frac{\omega}{2}(2t_a + t_e)\right] d\omega, \end{aligned} \quad (42)$$

which can be solved numerically and where K_ν is the modified Bessel function (see Appendix A). The results of the

integration with the parameters of a specific interferometer setup are given in Sec. VI [Fig. 4(a)].

2. Induced dipole of a microparticle

If the dipole is induced by the electric field of an external charge q_{ext} , its magnitude is given by [71,72]

$$\mathbf{d}_{\text{int}}^{(i)} = \frac{\epsilon_r - 1}{\epsilon_r + 2} \frac{q_{\text{ext}} R^3}{r^2(t)} \hat{\mathbf{r}}, \quad (43)$$

with the relative permittivity $\epsilon_r \approx 5.7$ for diamond and R being the radius of the spherical diamond [the superscript (i) indicates the induced dipole]. The acceleration in the $\hat{\mathbf{x}}$

TABLE I. Summary of the dephasing equations, the results were presented in (from top to bottom) Eqs. (32), (34), (37) for the charged interferometer and Eqs. (42), (45), and (47) for the neutral interferometer. $f(\omega)$ denotes the sinusoidal part of the transfer function, i.e., $f(\omega) \equiv \sin^4\left(\frac{t_a\omega}{2}\right) \sin^2\left[\frac{\omega}{2}(2t_a + t_e)\right]$, α and β are the projection angles of the impact-parameter vector and velocity on the \hat{x} axis, respectively, and θ_0 and γ are the projection angles of the impact parameter vector and velocity on the \hat{z} axis, respectively. The scheme's geometry is shown in Fig. 2, and a detailed derivation is presented in Appendix A. Figures 3 and 4 show that the dephasing increases with increasing velocity and decreasing impact parameter.

Interaction notation	Dephasing expression
Charge – charge cc	$\Gamma_n^{cc} = \frac{q_{\text{int}}^2 q_{\text{ext}}^2 (\Delta x)^2}{\pi^3 \hbar^2 \epsilon_0^2 v^4 t_a^4} \int_{\omega_{\text{min}}}^{\infty} \omega^{-4} [\cos^2(\alpha) K_1^2\left(\frac{b\omega}{v}\right) + \cos^2(\beta) K_0^2\left(\frac{b\omega}{v}\right)] f(\omega) d\omega$
Charge – permanent dipole cd(p)	$\Gamma_n^{\text{cd(p)}} = \frac{q^2 \mathbf{d}_{\text{ext}} ^2 (\Delta x)^2}{2\pi^2 \hbar^2 \epsilon_0^2 v^5 b t_a^4} \int_{\omega_{\text{min}}}^{\infty} \omega^{-3} [\cos^2(\alpha) K_{3/2}^2\left(\frac{b\omega}{v}\right) + \cos^2(\beta) K_{1/2}^2\left(\frac{b\omega}{v}\right)] f(\omega) d\omega$
Charge – induced dipole cd(i)	$\Gamma_n^{\text{cd(i)}} = \frac{q^4 \alpha_{\text{pol}}^2 (\Delta x)^2}{512\pi^4 \hbar^2 \epsilon_0^2 v^7 b^3 T t_a^4} \int_{\omega_{\text{min}}}^{\infty} \omega^{-1} [\cos^2(\alpha) K_{5/2}^2\left(\frac{b\omega}{v}\right) + \cos^2(\beta) K_{3/2}^2\left(\frac{b\omega}{v}\right)] f(\omega) d\omega$
Permanent dipole – charge d(p)c	$\Gamma_n^{\text{d(p)c}} = \frac{4q_{\text{ext}}^2 \mathbf{d}_{\text{int}} ^2 (\Delta x)^2}{9\pi^3 \epsilon_0^2 \hbar^2 v^6 t_a^4} \int_{\omega_{\text{min}}}^{\infty} \omega^{-2} (\cos^2(\alpha) [K_2^2\left(\frac{b\omega}{v}\right) \cos^2(\theta_0) + K_1^2\left(\frac{b\omega}{v}\right) \cos^2(\gamma)] + \cos^2(\beta) \{K_1^2\left(\frac{b\omega}{v}\right) \cos^2(\theta_0) + [\frac{b\omega}{v} K_1\left(\frac{b\omega}{v}\right) - K_0\left(\frac{b\omega}{v}\right)]^2 \cos^2(\gamma)\}) f(\omega) d\omega$
Induced dipole – charge d(i)c	$\Gamma_n^{\text{d(i)c}} = \left[\frac{\epsilon_r - 1}{\epsilon_r + 2}\right]^2 \frac{q_{\text{ext}}^4 R^6 (\Delta x)^2}{32\pi^2 \epsilon_0^2 \hbar^2 v^7 b^3 T t_a^4} \int_{\omega_{\text{min}}}^{\infty} \omega^{-1} [\cos^2(\alpha) K_{5/2}^2\left(\frac{b\omega}{v}\right) + \cos^2(\beta) K_{3/2}^2\left(\frac{b\omega}{v}\right)] f(\omega) d\omega$
Dipole – dipole dd	$\Gamma_n^{\text{dd}} = \frac{4 \mathbf{d}_{\text{ext}} ^2 \mathbf{d}_{\text{int}} ^2 (\Delta x)^2 \cos^2(\theta_0)}{\pi^3 \hbar^2 \epsilon_0^2 b^2 v^6 T t_a^4} \int_{\omega_{\text{min}}}^{\infty} \omega^{-2} [\cos^2(\alpha) K_2^2\left(\frac{b\omega}{v}\right) + \cos^2(\beta) K_1^2\left(\frac{b\omega}{v}\right)] f(\omega) d\omega$

direction then becomes

$$a_x^{\text{d(i)c}}(t) = \frac{\epsilon_r - 1}{\epsilon_r + 2} \frac{q_{\text{ext}}^2 R^3}{2\pi \epsilon_0 m b^5} \frac{\cos(\alpha) + (vt/b) \cos(\beta)}{[1 + (vt/b)^2]^3}. \quad (44)$$

The dephasing parameter is derived in detail in Appendix A, and is given by

$$\begin{aligned} \Gamma_n^{\text{d(i)c}} &= \left(\frac{\epsilon_r - 1}{\epsilon_r + 2}\right)^2 \frac{q_{\text{ext}}^4 R^6 (\Delta x)^2}{32\pi^2 \epsilon_0^2 \hbar^2 v^7 b^3 T t_a^4} \int_{\omega_{\text{min}}}^{\infty} \frac{1}{\omega} \\ &\times \left[\cos^2(\alpha) K_{5/2}^2\left(\frac{b\omega}{v}\right) + \cos^2(\beta) K_{3/2}^2\left(\frac{b\omega}{v}\right) \right] \\ &\times \sin^4\left(\frac{t_a\omega}{2}\right) \sin^2\left[\frac{\omega}{2}(2t_a + t_e)\right] d\omega, \quad (45) \end{aligned}$$

and K_ν is the modified Bessel function (see Appendix A). Again, this expression can be solved numerically to obtain the dephasing. The results of the integration with the parameters of a specific interferometer setup are given in Sec. VI [Fig. 4(b)]. Equation (45) differs from the permanent dipole result in Eq. (42) since the induced dipole is assumed to be induced by the external charge. As a result, Eq. (45) depends on the external charge and the relative permittivity and radius of the interferometer. The magnitude of the induced dipole is distance-dependent, resulting in a different v, b dependence of Eq. (45) compared with the permanent dipole dephasing result of Eq. (42).

B. Dephasing due to internal dipole and external dipole

The acceleration from the dipole-dipole interaction was given in Eq. (29). For large r , we can see that the other interactions dominate this interaction since it goes as $1/r^4$. Sticking with the assumptions made in previous sections, that \mathbf{d}_{ext} aligns with the \hat{z} direction, and that for a short interaction time τ , \mathbf{d}_{int} approximately aligns with $\hat{r}(t)$, the acceleration in the \hat{x} direction is

$$a_x^{\text{dd}}(t) = \frac{6|\mathbf{d}_{\text{ext}}||\mathbf{d}_{\text{int}}| \cos(\theta_0) \cos(\alpha) + (vt/b) \cos(\beta)}{4\pi \epsilon_0 m b^4 [1 + (vt/b)^2]^{5/2}}. \quad (46)$$

More details are given in Appendix A, where the Fourier transform of the acceleration and the resulting PSD is given. From the PSD and the transfer function, the dephasing is found to be

$$\begin{aligned} \Gamma_n^{\text{dd}} &= \frac{4|\mathbf{d}_{\text{ext}}|^2 |\mathbf{d}_{\text{int}}|^2 (\Delta x)^2 \cos^2(\theta_0)}{\pi^3 \hbar^2 \epsilon_0^2 b^2 v^6 T t_a^4} \int_{\omega_{\text{min}}}^{\infty} \frac{1}{\omega^2} \\ &\times \left[\cos^2(\alpha) K_2^2\left(\frac{b\omega}{v}\right) + \cos^2(\beta) K_1^2\left(\frac{b\omega}{v}\right) \right] \\ &\times \sin^4\left(\frac{t_a\omega}{2}\right) \sin^2\left[\frac{\omega}{2}(2t_a + t_e)\right] d\omega, \quad (47) \end{aligned}$$

see Appendix A for the detailed derivation. However, the result is an approximation given the assumptions made on this setup's dipole moments and velocities. Reference [50] provides a more general expression of the decoherence due to dipole-dipole interactions for spatial interferometers. The results of the integration with the parameters of a specific interferometer setup are given in Sec. VI [Fig. 4(c)].

VI. DEPHASING RESULTS

The dephasings found in this paper are summarized in Table I. The dephasing expressions are plotted in Figs. 3 and 4, which show that the dephasing increases for increasing velocity and decreasing impact parameter. The dephasing expressions show a solid inverse velocity dependence, but there is also a velocity dependence inside the integral part, which has been solved numerically to obtain the figures. Therefore, from the results in the table, it is tricky to draw any conclusions about physics. First, we discuss the dephasing for the charged microparticle, discussed in Secs. IV. They are plotted in Fig. 3. Here, we specify the experimental parameters and summarize the dipole moment orientation and evolution assumptions. The dephasing that is plotted is given in Eqs. (32), (34), and (37) corresponding to dephasing in a charged interferometer. We also discuss the possibility of the charged interferometer being an ideal quantum sensor to detect another electromagnetically charged particle moving in the vicinity.

The dephasing has been integrated in the frequency range from $\omega_{\min} = 2\pi/(t_f - t_i)$ to $\omega = \infty$. The experiment time is set to be $\tau = t_f - t_i = 4t_a + t_e$ (see Fig. 1). This frequency cutoff is chosen due to the frequency resolution of the discrete Fourier transform for the experimental setup. For the QGEM-specific example, we take $\tau \approx 1$ s; for the CNOT gate, we take $\tau \approx 1$ μ s.

These parameters are chosen such that no acceleration jitter can be averaged beyond the experimental time. We also optimized the projection angles, see Figs. 7–9, and the discussion in Appendix B. We have chosen the projection angles such that they maximize the dephasing. This will enable us to gauge the maximum acceleration noise the matter-wave interferometer can tolerate due to EM interactions. Also, it will help us do the total noise budget for the QGEM-type experiment [17] and with the charged microparticles [13].

We have also plotted the dephasing given in Eqs. (42), (45), and (47) relating to the neutral microparticle, which we discuss below. While plotting this dephasing for the neutral microparticle, we made the following additional assumptions for the dipoles to obtain approximately the upper bounds on the dephasing. (1) In Eq. (34), the external dipole is assumed to align approximately with the vector $\hat{r}(t)$ during the time of the experiment τ . (2) In Eq. (42) the interferometer dipole is assumed to align with the \hat{z} axis. (3) In Eq. (47) we assumed both the above assumptions.

Other relevant parameters we have set are the maximum superposition size of $\Delta x = 20$ μ m and $t_a = 0.50$ s and $t_e = 1.00$ s with total time $\tau = 3$ s. Furthermore, we have taken the timescale over which the noise is averaged, $T \sim b/v > 3$ s. We have also varied T in Fig. 4(a) for the neutral case for illustration.

A. Dephasing of a charged microparticle

As it is clear from the plots for the case of a charged microparticle interferometer, the dephasing depends on the particle's velocity v , and minimum impact parameter, which we take to be $b = 10$ – 100 μ m. For our analysis to be valid, the ambient particle is expected to have a small velocity $v \ll c$ since we have excluded relativistic effects in the potentials. In Fig. 3(a), the dephasing grows as the velocity increases for a fixed b . The charge-charge case dominates the dephasing over other cases. This can be seen from Fig. 3(d). The Coulomb interaction is by far the most dominant source of dephasing for the charged interferometer; see Figs. 3(a)–3(d). The charged interferometer can be treated as an excellent quantum sensor, sensing a charged ion moving with a velocity range of order $v \approx O(10^{-1})$ m/s in the vicinity of $b \approx 1$ m from the matter-wave interferometer (outside the range shown in the plot).

The dephasing due to charge-dipole interaction is shown in Figs. 3(b) and 3(c). Figure 3(b) shows the charged microparticle interacting with a molecule with a dipole interaction, where the external dipole is intrinsic to the external particle, for example, in a water molecule. The figure is plotted for a permanent dipole moment $|\mathbf{d}_{\text{ext}}| \approx 6.17 \times 10^{-30}$ Cm of a water molecule [73], with $b = 100$ μ m. The dephasing is plotted as a function of the velocity of the external water molecule. For smaller velocities, the dephasing is small, but as the velocity increases, the dephasing increases and it also

increases with the charge of the microparticle in the interferometer. We can see that the dephasing is small compared with the dephasing due to the Coulomb interaction.

Figure 3(c) shows the dephasing due to the charged microparticle and a dipole interaction where the external dipole is induced, for example, in the polarized air molecules. In this figure, we have taken the polarizability of dinitrogen, $(1.710 \text{ \AA}^3 = 1.903 \text{ \AA}^2 \text{ s}^4 \text{ kg}^{-1})$, which is most frequently present air molecule, and impact parameter $b = 30$ μ m. Again, the dephasing is negligible.

We summarize our results in Fig. 3(d), which shows the dephasings due to charge-charge (cc), charge-permanent dipole [cd(p)] and charge-induced dipole [cd(i)] as a function of the impact parameter b for $v = 1$ μ m s $^{-1}$. The plot shows how the impact parameter b influences dephasing in a fixed velocity scenario.

B. Dephasing of a neutral microparticle

In the case of a neutral interferometer, the results are shown in Fig. 4. Figure 4(a) shows the dephasing due to the interaction of an intrinsic dipole of a microparticle aligned at the \hat{z} axis interacting with an external charge. We have taken the external particle to have the charge of an electron. Following the analysis in Appendix B, where we have chosen the angles to maximize the dephasing, the projection angles are considered $\alpha = \beta = \pi/2$. Furthermore, as an example, we take the impact parameter $b = 100$ μ m. In this plot, we also show different values of the $T \sim b/v$ parameter to show how the dephasing behaves with varying interaction times. As the velocity increases for a fixed impact parameter, the dephasing increases. Nevertheless, the dephasing remains very small for our analysis to be valid $T = b/v > \tau = 3$ s.

Figure 4(b) shows the dephasing due to the interaction between an external charge and the dipole it induces within the diamond microsphere. We varied the mass of the microdiamond by changing the radius from $R \approx 1$ – 0.01 μ m, and the dielectric constant of the diamond is taken to be $\epsilon_r = 5.7$. The figure is very similar to Fig. 4(a), but the dephasing is significantly smaller (the plot is made for the impact parameter, $b = 100$ μ m). The dephasing would be further suppressed for smaller radii of the interferometer particle. In this case, the maximal projection angles were $\alpha = \beta = 0$, which would maximize the dephasing; see Appendix B.

The dephasing due to the dipole-dipole interaction is given in Fig. 4(c). Again, the interferometer is assumed to have a dipole aligned with the \hat{z} axis of magnitude $|\mathbf{d}_{\text{int}}| \approx 0.1 e \mu\text{m} \approx 1.6 \times 10^{-26}$ Cm. The external dipole is assumed to be that of water, $|\mathbf{d}_{\text{ext}}| \approx 6.17 \times 10^{-30}$ Cm. Following the analysis in Appendix B the projection angles are taken to be $\alpha = \beta = \pi/2$, which gives the maximum dephasing, e.g., worst-case scenario, if $vt/b < 1$. Different lines are shown for different impact parameters; one can see the dephasing is tiny.

It is worth pointing out that Ref. [50] also studied the decoherence due to the dipole-dipole interactions in approximately the same parameter space. Specifically, the paper found the decoherence rate using the scattering model in the Born-Markov approximation. A direct comparison may not be valid, as the authors considered a quantum bath consisting of particles modeled as plane waves inside a box. In contrast,

this paper considers a single external particle with classical trajectories. Still, comparing our analysis with the analysis from Ref. [50] is interesting. As the underlying assumptions are different, the predictions will, in general, differ, but a comparison nonetheless showed that when the impact factor b from this analysis matches the size of the particle R (and setting the number density corresponding to one environmental particle), the two predictions give the same order of magnitude prediction as expected (i.e., we match the length scale characterizing the distance between the system and environment to the same value in the two models).

Finally, Fig. 4(d) gives an overview of the dephasings described in Figs. 4(a)–4(c) as a function of the superposition width, showing that a smaller superposition width reduces the dephasing. The most dominant source of dephasing is from the permanent dipole interacting with an external (electron) charge for $b = 100 \mu\text{m}$ and $v = 10 \mu\text{ms}^{-1}$, which ensures $T \sim b/v > \tau$. The dephasing in all the cases is negligible.

VII. APPLICATIONS

We have discussed above the dephasing expressions for the charged and the neutral interferometers due to external charges and dipoles. We now discuss the applications for both cases. The neutral interferometer is discussed in the context of the QGEM proposal for testing the quantum nature of gravity by witnessing the spin entanglement [17]. We also discuss the charged interferometer in the context of an ion-based quantum computer (where entanglement is due to the interaction of the photon between the two ions in adjacent ion traps) and study the dephasing due to the external charge and dipoles for a setup similar to the QGEM case.

A. Protocol for quantum gravity-induced entanglement of masses

In the context of the QGEM protocol, details on which can be found here [17], we consider two neutral interferometers

that are set up in a way such their spatial superposition directions are parallel [41,42,77–79]. For illustration, the paths of a single spatial interferometer are assumed to be as illustrated in Fig. 1. The initial spin state of the interferometers is given by

$$|\psi(0)\rangle = \frac{1}{2}(|\uparrow\rangle_1 + |\downarrow\rangle_1) \otimes (|\uparrow\rangle_2 + |\downarrow\rangle_2), \quad (48)$$

which is a separable state (see Sec. II for a short discussion on how the spin degrees of freedom are used to create spatial superposition states and recombine the interferometric paths). A quantum gravitational interaction between the two massive interferometers will cause an entangling phase [17,21,22,24,26–28,80–83].

To simplify the analysis, we take the dephasing to be the same for both interferometers. Taking into account the dephasing of the two interferometers, the final wave function at a time $t = \tau$ is described by

$$|\psi(\tau)\rangle = \frac{e^{i\phi} e^{-i\delta\phi}}{2} (e^{i\delta\phi} |\uparrow\rangle_1 |\uparrow\rangle_2 + e^{i\Delta\phi} |\uparrow\rangle_1 |\downarrow\rangle_2 + e^{i\Delta\phi} |\downarrow\rangle_1 |\uparrow\rangle_2 + e^{-i\delta\phi} |\downarrow\rangle_1 |\downarrow\rangle_2), \quad (49)$$

with

$$\phi = \frac{\tau}{\hbar} \frac{Gm^2}{d}, \quad \Delta\phi = \frac{\tau}{\hbar} \int_0^\tau \frac{Gm^2}{\sqrt{d^2 + \Delta x^2(t)}} dt - \phi, \quad (50)$$

where $\delta\phi$ is the phase difference between the left and right arm of the interferometer due to interaction with the environmental particle, see Eq. (1).

The density matrix ρ is given by the final wave function, $\rho = |\psi\rangle\langle\psi|$. Averaging over the different runs of the experiment, we find $\mathbb{E}[\rho]$. Treating $\delta\phi$ as a statistical quantity with $\mathbb{E}[\delta\phi] = 0$ as discussed in Sec. II, and $\mathbb{E}[(\delta\phi)^2] = \Gamma_n$, see Eq. (9), the averaged density matrix is given by⁷

$$\mathbb{E}[\rho] = \frac{1}{4} \begin{pmatrix} 1 & e^{-\Gamma_n/2 - i\Delta\phi} & e^{-\Gamma_n/2 - i\Delta\phi} & e^{-2\Gamma_n} \\ e^{-\Gamma_n/2 + i\Delta\phi} & 1 & 1 & e^{-\Gamma_n/2 + i\Delta\phi} \\ e^{-\Gamma_n/2 + i\Delta\phi} & 1 & 1 & e^{-\Gamma_n/2 + i\Delta\phi} \\ e^{-2\Gamma_n} & e^{-\Gamma_n/2 - i\Delta\phi} & e^{-\Gamma_n/2 - i\Delta\phi} & 1 \end{pmatrix}. \quad (51)$$

Γ_n is given by the results found in the previous sections for the neutral microparticle. To witness the entanglement due to the gravitational interaction, we use the positive partial transpose (PPT) witness, which, in the case of two qubits, provides a sufficient and necessary condition for entanglement based on the Peres-Horodecki criterion [16,41,42]. The PPT witness is defined as $\mathcal{W} = |\lambda_- \rangle \langle \lambda_-|^T$, where $|\lambda_- \rangle$ is the eigenvector corresponding to the lowest eigenvalue, λ_- , of the partially transposed density matrix and the super-

script T_2 denotes the partial transpose over system 2. The witness for two interferometers aligned in a parallel way, corresponding to the wave function in Eq. (49), was found to be [77]

$$\mathcal{W} = \frac{1}{4} (1 \otimes 1 - \sigma_x \otimes \sigma_x + \sigma_z \otimes \sigma_y + \sigma_y \otimes \sigma_z), \quad (52)$$

with $\sigma_x, \sigma_y, \sigma_z$ being the Pauli spin matrices. The expectation value of the witness is given by [41,42,78]

$$\langle \mathcal{W} \rangle = \text{Tr}(\mathcal{W}\rho) = \lambda_-. \quad (53)$$

For the wave function in Eq. (49) the expectation value is found to be

$$\langle \mathcal{W} \rangle = \frac{1}{8} (1 - e^{-2\Gamma_n}) - \frac{1}{2} \sin(|\Delta\phi|) e^{-\Gamma_n/2}, \quad (54)$$

⁷Here we have used that $\mathbb{E}[e^{i\delta\phi}] \approx e^{-\mathbb{E}[(\delta\phi)^2]/2}$, assuming $\delta\phi$ follows a Gaussian distribution with $\mathbb{E}[\delta\phi] = 0$ [84].

which reduces to the witness expectation value in Ref. [77] if $\Gamma_n = 0$. The entanglement detection condition is $\langle \mathcal{W} \rangle < 0$. There is no entanglement detection if $\langle \mathcal{W} \rangle \geq 0$. Performing a short-time expansion of the witness, these inequalities can approximate the maximum allowed value of the dephasing rate:

$$2\Gamma_n - \frac{|\Delta\phi|}{2} < 0. \quad (55)$$

In particular, if $\Gamma_n > |\Delta\phi|/4$, then $\langle \mathcal{W} \rangle > 0$ and there is no entanglement. Hence, the total dephasing due to the EM interaction must be $\Gamma_n < |\Delta\phi|/4$ to detect the gravity-induced entanglement.

We now consider the induced dipole-charge and the dipole-dipole dephasing [Eqs. (45) and (47), respectively]. To simplify the analysis, we consider the gas temperatures to be small ($T \approx 0.1$ mK) such that the Maxwell-Boltzmann distribution in Eq. (19) can be approximated with a Dirac-delta distribution around the velocity $\bar{v} = \sqrt{2k_B T_{\text{gas}}/m_{\text{gas}}}$, with $m_{\text{gas}} = 4.8 \times 10^{-26}$ kg corresponding to the typical mass of an air molecule. We further simplify the analysis by considering only the dominant frequency mode $\omega = \omega_{\text{min}}$, allowing for an approximation of the Bessel function (see the last three rows of Table I). These approximations are detailed and motivated in Appendix C. Furthermore, the timescale T is taken to be larger than the experimental time, $T = 10\tau$, such that Eq. (4) holds.

In the context of the QGEM experiment, we consider the diamond to have a relative permittivity of $\epsilon_r = 5.1$ [77,85], and mass $m = 10^{-15}$ kg. We further assume that the maximum superposition size is $\Delta x = 10 \mu\text{m}$ and that the total time is $\tau = 1$ s and the superposition is created following the scheme in Fig. 1. The transfer function of the interferometer is given Eq. (13), where the times t_e, t_a are scaled-down compared with previous figures such that the total experimental time is 1 s. For the external particle, we have taken the same properties as in Fig. 4(a)–4(d).

The dephasing from the dipole-dipole interaction for the QGEM experiment is shown in Fig. 5, where we have assumed an external dipole of magnitude $|\mathbf{d}_{\text{ext}}| = 6.17 \times 10^{-30}$ Cm, and the interferometer dipole is assumed to be $|\mathbf{d}_{\text{int}}| = 10^{-7} e$ Cm. The figure shows the total dephasing as a function of the number density of gas particles in a square box of size $L = 0.01$ cm cooled to $T_{\text{gas}} = 0.1$ mK. The dephasing in Fig. 5 considers multiple particles described by a distribution over velocities, impact parameters and projection angles. Although remnant charges would cause a deleterious dephasing in the QGEM experiment, remnant dipoles within the vacuum chamber for the number density shown in Fig. 5 have a dephasing such that the entanglement remains witnessable.

B. CNOT gate

In quantum computers, one often considers trapped charged particles [59,60]. Here, we consider a CNOT gate consisting of two trapped ions separated by a distance d . Their initial wave function will be assumed to be prepared in a product state consisting of individual spatial superpositions. The entanglement between the two trapped ions will then build

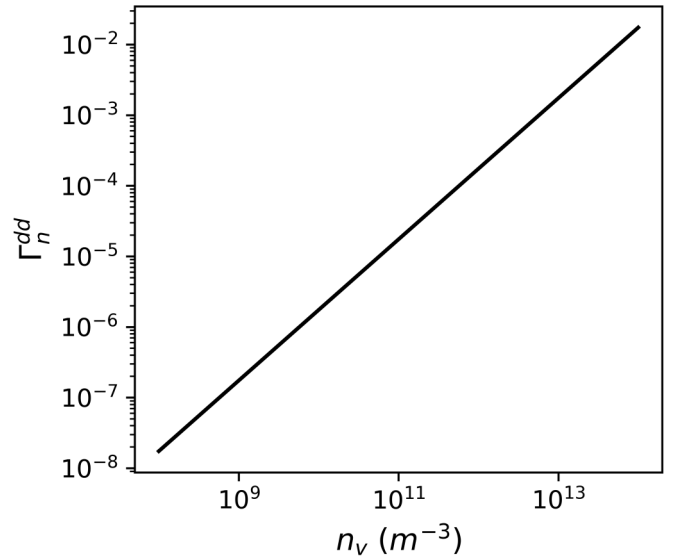


FIG. 5. Dephasing for the QGEM microdiamond setup [77] as a function of number density $n_v \in [10^8 \text{ m}^{-3}, 10^{14} \text{ m}^{-3}]$, in a square box of size $L = 0.01$ m. We consider the diamond to have a permanent dipole of $0.1 e \mu\text{m}$, and mass $m = 10^{-15}$ kg. The external gas particles are assumed to have a dipole similar to that of a water molecule with the distributions given in Eqs. (18)–(21) and the temperature $T_{\text{gas}} = 0.1$ mK. We further assume that the maximum superposition size is $\Delta x = 10 \mu\text{m}$ and that the total interferometric time is $\tau = 1$ s. The dephasing is from the dipole-dipole interaction, see Fig. 4(c), now applied to the QGEM parameters and taking only the dominant frequency mode $\propto 1/\tau$ into account.

up due to the EM interaction mediated via photon, essentially the Coulomb interaction. The final wave function of such an entangled system will be given by Eq. (49), with an entangled phase given by

$$\Delta\phi = -\frac{\tau}{\hbar} \int_0^\tau \frac{\kappa_e q_1 q_2}{\sqrt{d^2 + \Delta x^2(t)}} dt - \phi, \quad (56)$$

$$\text{with } \phi = -\frac{\tau}{\hbar} \frac{\kappa_e q_1 q_2}{d}, \quad (57)$$

where $\kappa_e = (4\pi\epsilon_0)^{-1}$, and q_1 and q_2 are internal charges of the ions in their respective traps.

In Fig. 6, we show the dephasing Γ_n^{cc} from the charge-charge Coulomb interaction. We have assumed that an external charge $q_{\text{ext}} = 10e$ (which is not trapped) is flying by the ion traps. We assume for simplicity that each trapped ion has mass $m \approx 10^{-27}$ kg, charge $q_{\text{int}} = q_1 = q_2 = e$ and is trapped in a trap of frequency $\omega = 10^5$ Hz. For concreteness, we can consider the size of the superposition size to be of the same order of magnitude as the zero point motion $\Delta x = \sqrt{\hbar/2m\omega}$, which for our parameters gives $\Delta x \approx 0.18 \mu\text{m}$. The entanglement builds up swiftly due to the Coulomb interaction, which is many orders of magnitude larger than the gravitational interaction strength. The total experimental time we require is $\tau = 1 \mu\text{s}$ for the entanglement phase to be order unity assuming a trap separation $d = 50 \mu\text{m}$. For illustration, we took a similar transfer function responsible for creating the spatial superposition in Fig. 1.

The dephasing in Fig. 6 has been found for multiple gas particles that have velocity, impact parameter and projection

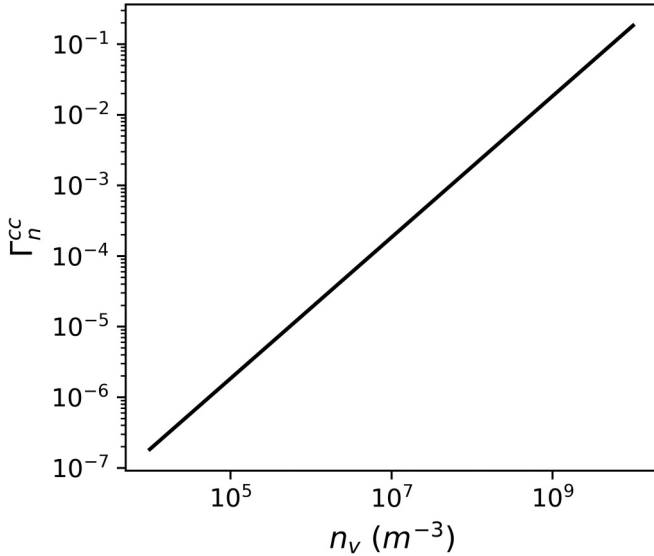


FIG. 6. Charge-charge dephasing for ions of mass $m = 10^{-27}$ kg and total charge $q_{\text{int}} = e$ interacting with an external particle of charge $q_{\text{ext}} = 10e$ as a function of the number density $n_v \in [10^4 \text{ m}^{-3}, 10^{10} \text{ m}^{-3}]$ in a square box of size $L = 0.01$ m. The experimental time is $\tau = 1 \mu\text{s}$ and the superposition size is assumed to be $\Delta x = 0.18 \mu\text{m}$. The dephasing is approximated for temperatures $T_{\text{gas}} = 0.1$ mK and $b_{\text{min}} \approx 10^{-7}$ m.

angles following the distributions in Eqs. (18)–(21). The dephasing is approximated by imposing a minimal impact parameter $b \in [b_{\text{min}}, L]$ with $b_{\text{min}} = 10^3 R \approx 10^{-7}$ m and $L = 0.01$ m, such that a large-argument expansion can be used to approximate the Bessel function. This approximation is detailed in Appendix C. Figure 6 shows the dephasing as a function of the number density such that the dephasing is smaller than the entanglement phase. Note that the simplifying assumptions for the CNOT gate are slightly different compared with the QGEM experiment because the two experimental setups have different experimental parameters, we refer to Appendix C for more detail.

VIII. CONCLUSION

In this paper, we have adapted techniques from investigating noninertial and gravitational noise [51,55,56] to compute the dephasing arising from the electromagnetic interactions. We considered two distinct scenarios, one where the interferometer particle is charged and the other where the micron-size particle is neutral. The main formulas are summarized in Table I.

The charged interferometer can interact via Coulomb interaction with an external charged particle. The external particle’s velocity is assumed to be constant, and its acceleration on both arms of the interferometer causes a jitter, which causes dephasing. The charged interferometer can also interact with a constantly moving dipole. The ambient particle can have a permanent dipole or an induced dipole. We considered both cases separately; see Figs. 3(a)–3(d). The largest dephasing occurs due to the Coulomb interaction, which sets the exclusion zone for an externally charged particle.

In the neutral case, we have again four possibilities; a microparticle is typically considered a diamond in our case, which has a dielectric property. The microdiamond can then have a permanent and an induced dipole; hence, it can interact with an external charge and an external dipolar particle, see Figs. 4(a)–4(d). The external particle will impart a jitter in the trajectories due to the relative accelerations of the arms of the matter wave interferometer and, hence, will induce a dephasing.

Suppose two neutral microparticles, each prepared in spatial superpositions and kept in adjacent locations as in the case of the QGEM experiment [17]. In that case, the relative acceleration noise is present in both test masses. This will cause a dephasing, as shown in Fig. 5, leading to entanglement degradation. The approximate average dephasing was found considering the probability distributions in Eqs. (18)–(21). We found that it requires $\Gamma_n < |\Delta\phi|/4$, with Γ_n denoting the dephasing and $2\Delta\phi$ the entanglement phase, to witness entanglement in the QGEM setup (positive partial trace witness [41,42,78]). In the QGEM-type experiment, the dephasing from the external jitters due to the dipole-dipole interactions is small enough for the parameter space considered in this paper. At the same time, the dipole-charge interactions cause too much jitter.

The relative acceleration noise can also affect the ion trapped spatial qubits, forming a CNOT gate. We observed that our methodology could be successfully employed to characterize the electromagnetic noise for such a setup. We found that the average dephasing, considering the probability distributions in Eqs. (18)–(21), increases as shown in Fig. 6. The developed methodology could thus be used to estimate the decoherence budget.

However, our analysis has also its limitations, which is suggestive for a more refined modeling in future works. We were able to obtain analytical results by assuming that the trajectories of the external particles are approximately classical and that the dynamics is nonrelativistic. We also supposed that the ensemble of external particles is characterized by flat distribution of angles, impact parameters, and a Gaussian distribution in the velocities. While the modeling seem to be plausible from the experimental perspective, the analysis could be further refined with the help of numerical packages as analytical calculations will likely become challenging.

In summary, we have provided a way of characterizing electromagnetic sources of dephasing due to external particles in the context of matter-wave interferometry. The developed techniques can be applied in fundamental problems such as witnessing the quantum nature of gravity in a laboratory, and it could find applications for the design of future ion-based quantum computers.

ACKNOWLEDGMENTS

The Fundamentals of the Universe research program at the University of Groningen supports M.S. M.T. acknowledges funding by the Leverhulme Trust (RPG-2020-197). S.B. would like to acknowledge EPSRC grants (EP/N031105/1, EP/S000267/1, and EP/X009467/1) and grant ST/W006227/1. S.B. and A.M. research is supported by the Sloan, and Betty and Moore foundations.

APPENDIX A: ESTIMATION OF DEPHASING

This section shows the expressions for the Fourier transform of the acceleration $a_x(\omega)$ and the corresponding PSD for the acceleration noise $S_{aa}(\omega)$, from which the dephasing due to the acceleration noise can be derived via

$$\Gamma_n = \frac{1}{2\pi} \frac{m^2}{\hbar^2} \int_{\omega_{\min}}^{\infty} S_{aa}(\omega) F(\omega) d\omega, \quad (\text{A1})$$

with the transfer function $F(\omega)$ determined by the trajectory, see Eq. (13). Since

$$a(\omega) = \int_{-\infty}^{\infty} a(t) e^{-i\omega t} dt, \quad (\text{A2})$$

$$a(t) = \frac{1}{2\pi} \int_{-\infty}^{\infty} a(\omega) e^{i\omega t} d\omega. \quad (\text{A3})$$

We rewrite the acceleration such that the Fourier transform can easily be performed:

$$a(b\omega/v) = \frac{b}{v} \int_{-\infty}^{\infty} a(vt/b) e^{-i(b\omega/v)(vt/b)} d(vt/b). \quad (\text{A4})$$

The Fourier transform is of a function $f(vt/b)$ as defined below is given by

$$f(vt/b) = \frac{(vt/b)^{2n}}{[(vt/b)^2 + c^2]^{\nu+1/2}},$$

$$f(b\omega/v) = \frac{(-1)^n c^\nu \sqrt{\pi}}{2^\nu \Gamma(\nu + 1/2)} \frac{\partial^{2n}(b\omega/v)^\nu K_\nu(cb\omega/v)}{\partial(b\omega/v)^{2n}}, \quad (\text{A5})$$

with $\Gamma(x)$ the Euler-Gamma function⁸ and K_ν the modified Bessel function of the second kind with order ν . The above Fourier transform holds only if $\text{Re}(c) > 0$ and $\text{Re}(\nu + 1/2) > n$. The modified Bessel functions have the property that

$$\frac{\partial K_\nu(x)}{\partial x} = -\frac{1}{2} [K_{\nu-1}(x) + K_{\nu+1}(x)],$$

$$K_{\nu-1}(x) = K_{\nu+1}(x) - \frac{2\nu}{x} K_\nu(x). \quad (\text{A6})$$

The modified Bessel functions with half integers have the analytic formula

$$K_{1/2}(u) = \sqrt{\frac{\pi}{2u}} e^{-u},$$

$$K_{3/2}(u) = \sqrt{\frac{\pi}{2u}} \left(1 + \frac{1}{u}\right) e^{-u},$$

$$K_{5/2}(u) = \sqrt{\frac{\pi}{2u}} \left(1 + \frac{3}{u} + \frac{3}{u^2}\right) e^{-u}. \quad (\text{A7})$$

The integer-modified Bessel functions of the second kind do not have an analytical formula but can be expressed in the

⁸With relevant values $\Gamma(3/2) = \sqrt{\pi}/2$, $\Gamma(2) = 1$, $\Gamma(5/2) = 3\sqrt{\pi}/4$, and $\Gamma(3) = 2$.

integral form

$$K_0(u) = \int_0^\infty \frac{\cos(tu)}{\sqrt{1+t^2}} dt,$$

$$K_1(u) = \frac{1}{u} \int_0^\infty \frac{\cos(tu)}{(1+t^2)^{3/2}} dt,$$

$$K_2(u) = \frac{3}{u^2} \int_0^\infty \frac{\cos(tu)}{(1+t^2)^{5/2}} dt. \quad (\text{A8})$$

1. Charge-charge interaction

As presented in Eq. (31), the acceleration due to the charge-charge interaction in the \hat{x} direction is

$$a_x^{\text{cc}}(t) = \frac{q_{\text{int}} q_{\text{ext}}}{4\pi \epsilon_0 m b^2} \frac{\cos(\alpha) + (vt/b) \cos(\beta)}{[1 + (vt/b)^2]^{3/2}}. \quad (\text{A9})$$

Transforming the acceleration $a_x^{\text{cc}}(t)$ into the frequency domain, we use Eq. (A5) (with $c = 1$, $\nu = 1$, $n = 0, 1/2$) to obtain

$$a_x^{\text{cc}}(\omega) = \frac{q_{\text{int}} q_{\text{ext}} \omega}{4\pi \epsilon_0 m v^2} \left[\cos(\alpha) K_1\left(\frac{b\omega}{v}\right) - i \cos(\beta) K_0\left(\frac{b\omega}{v}\right) \right], \quad (\text{A10})$$

where $K_\nu(x)$ is a modified Bessel function, and we used its properties in Eq. (A6). Note that after Fourier transform, the units of $a_x(\omega)$ are $\text{m}/(\text{s}^2 \text{ Hz})$, which is because $a_x(t) = \int a_x(\omega) e^{i\omega t} d\omega$ has units of m/s^2 and $d\omega$ has units of Hz.

Substituting Eq. (A10) for the acceleration due to the Coulomb interaction into Eq. (6) for the PSD results in the desired PSD of the acceleration noise from the Coulomb interaction:

$$S_{aa}^{\text{cc}}(\omega) = \frac{q_{\text{int}}^2 q_{\text{ext}}^2 \omega^2}{16\pi^2 T m^2 v^4 \epsilon_0^2} \left[\cos^2(\alpha) K_1^2\left(\frac{b\omega}{v}\right) + \cos^2(\beta) K_0^2\left(\frac{b\omega}{v}\right) \right]. \quad (\text{A11})$$

Note that the units of $S_{aa}(\omega) = |a_x(\omega)|^2/T$ are $\text{m}^2/(\text{s}^4 \text{ Hz})$. Using Eq. (A1) gives the dephasing in Eq. (32).

2. Charge-dipole interaction

a. Permanent dipole

As presented in Eq. (33), the acceleration due to the charge-permanent dipole interaction in the \hat{x} direction is

$$a_x^{\text{cd(p)}}(t) = \frac{q |\mathbf{d}_{\text{ext}}| \cos(\alpha) + (vt/b) \cos(\beta)}{2\pi m b^3 \epsilon_0 [1 + (vt/b)^2]^2}. \quad (\text{A12})$$

Transforming the acceleration $a_x^{\text{cd(p)}}(t)$ into the frequency domain, we use Eq. (A5) (with $c = 1$, $\nu = 3/2$, $n = 0, 1/2$) to obtain

$$a_x^{\text{cd(p)}}(\omega) = \frac{q |\mathbf{d}_{\text{ext}}| \omega^{3/2}}{4\pi \epsilon_0 m v^{3/2} b^{3/2}} \sqrt{\frac{\pi}{2}} \frac{b}{v} \left[\cos(\alpha) K_{3/2}\left(\frac{b\omega}{v}\right) - i \cos(\beta) K_{1/2}\left(\frac{b\omega}{v}\right) \right], \quad (\text{A13})$$

where $K_\nu(x)$ is a modified Bessel function, and we used its properties in Eq. (A6).

Now substituting this expression into the definition of the PSD of the acceleration noise results in

$$S_{aa}^{\text{cd(p)}}(\omega) = \frac{q^2 |\mathbf{d}_{\text{ext}}|^2 \omega^3}{32\pi T m^2 v^5 b \epsilon_0^2} \times \left[\cos^2(\alpha) K_{3/2}^2\left(\frac{b\omega}{v}\right) + \cos^2(\beta) K_{1/2}^2\left(\frac{b\omega}{v}\right) \right]. \quad (\text{A14})$$

The resulting dephasing is given in Eq. (34).

b. Induced dipole

As presented in Eq. (36), the acceleration due to the charge-permanent dipole interaction in the \hat{x} direction is

$$a_x^{\text{cd(i)}}(t) = \frac{q_{\text{int}}^2 \alpha_{\text{pol}}}{8\pi^2 m b^5 \epsilon_0^2} \frac{\cos(\alpha) + (vt/b) \cos(\beta)}{[1 + (vt/b)^2]^3}.$$

Performing a Fourier transform given in Eq. (A5) (with $c = 1$, $v = 5/2$, $n = 0, 1/2, 1$) to find the acceleration in the frequency domain gives

$$a_x^{\text{cd(i)}}(\omega) = \frac{q^2 \alpha_{\text{pol}} \omega^{5/2}}{64\pi^2 m b^3 v^7 \epsilon_0^2} \sqrt{\frac{\pi}{2}} \times \left[\cos(\alpha) K_{5/2}\left(\frac{b\omega}{v}\right) - i \cos(\beta) K_{3/2}\left(\frac{b\omega}{v}\right) \right]. \quad (\text{A15})$$

Substituting this expression into the definition of the PSD of the acceleration noise results in a slightly modified expression compared with the permanent dipole case:

$$S_{aa}^{\text{cd(i)}}(\omega) = \frac{q^4 \alpha_{\text{pol}}^2 \omega^5}{8192\pi^3 m^2 v^7 b^3 \epsilon_0^4 T} \times \left[\cos^2(\alpha) K_{5/2}^2(b\omega/v) + \cos^2(\beta) K_{3/2}^2(b\omega/v) \right]. \quad (\text{A16})$$

The resulting dephasing is given in Eq. (37).

3. Dipole-charge interaction

a. Permanent dipole

As presented in Eq. (41) the acceleration in the \hat{x} direction due to the permanent dipole interacting with an external charge is

$$a_x^{\text{d(p)c}}(t) = \frac{q_{\text{ext}} |\mathbf{d}_{\text{int}}| \cos(\alpha) + (vt/b) \cos(\beta)}{2\pi m b^3 \epsilon_0} \frac{1}{[1 + (vt/b)^2]^{5/2}} \times [\cos(\theta_0) + (vt/b) \cos(\gamma)], \quad (\text{A17})$$

The second line comes from the resolution of the dot product as

$$\mathbf{d}_{\text{int}} \cdot \hat{\mathbf{r}}(t) = |\mathbf{d}_{\text{int}}| \frac{b_z + v_z t}{r(t)} \quad (\text{A18})$$

$$= |\mathbf{d}_{\text{int}}| \frac{\cos(\theta_0) + (vt/b) \cos(\gamma)}{\sqrt{1 + (vt/b)^2}}, \quad (\text{A19})$$

where we have assumed that the direction of the dipole vector of the interferometer is constant, i.e., \mathbf{d}_{int} is not time

dependent, and that it points in the \hat{z} direction. For example, because the microdiamond sphere is magnetically trapped [40] and its rotational degrees of freedom are cooled to near its ground state [86], achieving good control of the system.

In the second line above, Eq. (A19) we have written the dot product in terms of the angle θ_0 , which is the angle between the \hat{z} axis and the vector b , and the angle γ which gives the \hat{z} component of the velocity:

$$b_z = b \cos(\theta_0), \quad v_z = v \cos(\gamma). \quad (\text{A20})$$

The Fourier transform of the acceleration $a_x^{\text{d(p)c}}(t)$ is found from Eq. (A5) (with $c = 1$, $v = 2$, $n = 0, 1/2, 1$) and gives

$$a_x^{\text{d(p)c}}(\omega) = \left(\cos(\alpha) \left[K_2\left(\frac{b\omega}{v}\right) \cos(\theta_0) - i K_1\left(\frac{b\omega}{v}\right) \cos(\gamma) \right] - i \cos(\beta) \left\{ K_1\left(\frac{b\omega}{v}\right) \cos(\theta_0) - i \left[\frac{b\omega}{v} K_1\left(\frac{b\omega}{v}\right) - K_0\left(\frac{b\omega}{v}\right) \right] \cos(\gamma) \right\} \right) \frac{q_{\text{ext}} |\mathbf{d}_{\text{int}}| \omega^2}{6\pi \epsilon_0 m v^3}, \quad (\text{A21})$$

where we used Eqs. (A5) to find the Fourier transform and Eqs. (A6) to simplify the expression.

Now substituting this expression into the Eq. (5) of the PSD of the acceleration noise results in

$$S_{aa}^{\text{d(p)c}}(\omega) = \frac{q_{\text{ext}}^2 |\mathbf{d}_{\text{int}}|^2 \omega^4}{36\pi^2 \epsilon_0^2 m^2 v^6 T} \left(\cos^2(\alpha) \left[K_2^2\left(\frac{b\omega}{v}\right) \times \cos^2(\theta_0) + K_1^2\left(\frac{b\omega}{v}\right) \cos^2(\gamma) \right] + \cos^2(\beta) \left\{ K_1^2\left(\frac{b\omega}{v}\right) \cos^2(\theta_0) + \left[\frac{b\omega}{v} K_1\left(\frac{b\omega}{v}\right) - K_0\left(\frac{b\omega}{v}\right) \right]^2 \cos^2(\gamma) \right\} \right).$$

The resulting dephasing from Eq. (A1) and (13) is given by

$$\Gamma_n^{\text{d(p)c}} = \frac{4q_{\text{ext}}^2 |\mathbf{d}_{\text{int}}|^2 (\Delta x)^2}{9\pi^3 \epsilon_0^2 \hbar^2 v^6 t_a^4} \int_{\omega_{\text{min}}}^{\infty} \frac{1}{\omega^2} \sin^4\left(\frac{t_a \omega}{2}\right) \times \left(\cos^2(\alpha) \left[K_2^2\left(\frac{b\omega}{v}\right) \cos^2(\theta_0) + K_1^2\left(\frac{b\omega}{v}\right) \cos^2(\gamma) \right] + \cos^2(\beta) \left\{ K_1^2\left(\frac{b\omega}{v}\right) \cos^2(\theta_0) + \left[\frac{b\omega}{v} K_1\left(\frac{b\omega}{v}\right) - K_0\left(\frac{b\omega}{v}\right) \right]^2 \cos^2(\gamma) \right\} \right) \sin^2\left[\frac{\omega}{2}(2t_a + t_e)\right] d\omega. \quad (\text{A22})$$

Which has been presented in Eq. (42) in a simplified form.

b. Induced dipole

Equation (44) gave the acceleration in the \hat{x} direction for the interaction between an external charge and the dipole it

induces in the interferometer:

$$a_x^{d(i)c}(t) = \frac{\epsilon_r - 1}{\epsilon_r + 2} \frac{q_{\text{ext}}^2 R^3 \cos(\alpha) + (vt/b) \cos(\beta)}{2\pi\epsilon_0 m b^5 [1 + (vt/b)^2]^3}. \quad (\text{A23})$$

Performing a Fourier transform to find the acceleration in the frequency domain gives (from Eq. (A5) with $c = 1$, $v = 5/2$, $n = 0, 1/2$):

$$a_x^{d(i)c}(\omega) = \frac{\epsilon_r - 1}{\epsilon_r + 2} \frac{q_{\text{ext}}^2 R^3 \omega^{5/2}}{16\pi m b^{5/2} v^{5/2} \epsilon_0} \frac{b}{v} \sqrt{\frac{\pi}{2}} \times \left[\cos(\alpha) K_{5/2}\left(\frac{b\omega}{v}\right) - i \cos(\beta) K_{3/2}\left(\frac{b\omega}{v}\right) \right]. \quad (\text{A24})$$

Substituting this expression into the PSD of the acceleration noise results in a slightly modified expression compared with the permanent dipole case:

$$S_{aa}^{d(i)c} = \left(\frac{\epsilon_r - 1}{\epsilon_r + 2} \right)^2 \frac{q_{\text{ext}}^4 R^6 \omega^5}{512\pi \epsilon_0^2 m^2 v^7 b^3 T} \times \left[\cos^2(\alpha) K_{5/2}^2\left(\frac{b\omega}{v}\right) + \cos^2(\beta) K_{3/2}^2\left(\frac{b\omega}{v}\right) \right], \quad (\text{A25})$$

from which Eq. (45) is derived.

4. Dipole-dipole interaction

The acceleration due to dipole-dipole interactions is given by [71]

$$\mathbf{a}_{dd} = \frac{3\hat{\mathbf{r}}}{4\pi\epsilon_0 m} \left[\frac{\mathbf{d}_{\text{ext}} \cdot \mathbf{d}_{\text{int}}}{r^4(t)} - 3 \frac{(\mathbf{d}_{\text{ext}} \cdot \hat{\mathbf{r}})(\mathbf{d}_{\text{int}} \cdot \hat{\mathbf{r}})}{r^4(t)} \right]. \quad (\text{A26})$$

To resolve the dot products, we recall from previous sections the assumption we made:

(1) The external particle has low velocity, meaning that $\mathbf{d}_{\text{ext}} \cdot \hat{\mathbf{r}}$ is approximately constant in time. Furthermore, in the worst-case scenario, $\mathbf{d}_{\text{ext}} \cdot \hat{\mathbf{r}} = |\mathbf{d}_{\text{ext}}|$.

(2) The dipole of the interferometer particle is aligned with the $\hat{\mathbf{z}}$ axis. Such that $\mathbf{d}_{\text{int}} \cdot \hat{\mathbf{r}}$ is as in Eq. (A19). Assuming that the external particle has small velocity, $\mathbf{d}_{\text{int}} \cdot \hat{\mathbf{r}} \approx |\mathbf{d}_{\text{int}}| \cos(\theta_0)$.

From the orientation of the dipoles in these assumptions, it follows that

(1) the angle between the interferometer and external dipoles is θ_0 , such that $\mathbf{d}_{\text{int}} \cdot \mathbf{d}_{\text{ext}} = |\mathbf{d}_{\text{int}}| |\mathbf{d}_{\text{ext}}| \cos(\theta_0)$.

In this scenario, the acceleration in the $\hat{\mathbf{x}}$ direction becomes

$$a_x^{dd}(t) = -\frac{6}{4\pi\epsilon_0 m} \frac{|\mathbf{d}_{\text{ext}}| |\mathbf{d}_{\text{int}}| \cos(\theta_0) r_x}{r^4(t)} = -\frac{6|\mathbf{d}_{\text{ext}}| |\mathbf{d}_{\text{int}}| \cos(\theta_0) \cos(\alpha) + (vt/b) \cos(\beta)}{4\pi\epsilon_0 m b^4 [1 + (vt/b)^2]^{5/2}},$$

as presented in Eq. (46). Using the Fourier transform in Eq. (A5) and the properties given in Eq. (A6) gives:

$$a_x^{dd}(\omega) = \frac{2|\mathbf{d}_{\text{ext}}| |\mathbf{d}_{\text{int}}| \cos(\theta_0) \omega^2}{4\pi\epsilon_0 m b v^3} \times \left[\cos(\alpha) K_2\left(\frac{b\omega}{v}\right) - i \cos(\beta) K_1\left(\frac{b\omega}{v}\right) \right], \quad (\text{A27})$$

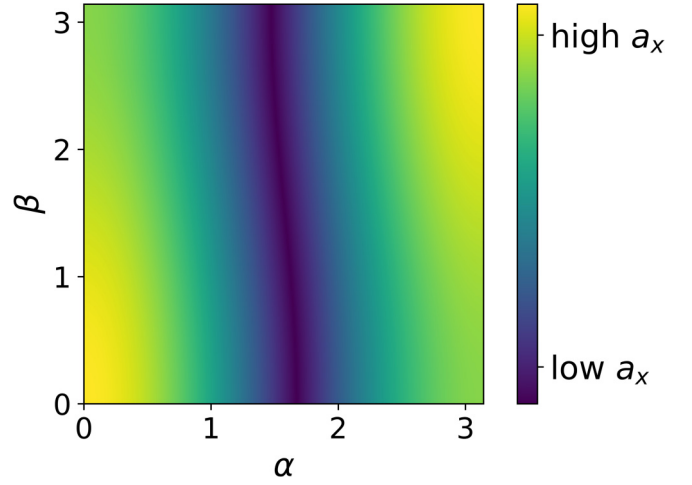


FIG. 7. For $vt/b = 0.1$ the absolute value of the acceleration [Eq. (B1) with $a = 3$] as a function of the projection angles $\alpha, \beta \in [0, \pi]$.

which gives the PSD of the acceleration noise:

$$S_{aa}^{dd}(\omega) = \frac{|\mathbf{d}_{\text{ext}}|^2 |\mathbf{d}_{\text{int}}|^2 \cos^2(\theta_0) \omega^4}{4\pi^2 \epsilon_0^2 m^2 T b^2 v^6} \times \left[\cos^2(\alpha) K_2^2\left(\frac{b\omega}{v}\right) + \cos^2(\beta) K_1^2\left(\frac{b\omega}{v}\right) \right]. \quad (\text{A28})$$

Together with the transfer function, this gives the dephasing due to the dipole-dipole interaction, as given in Eq. (47).

APPENDIX B: PROJECTION ANGLES ANALYSIS

To maximize the dephasing, we take the initial conditions as given by the projections angles α and β (respectively, b and v in the $\hat{\mathbf{x}}$ direction) and in the case of an interferometer dipole θ_0 and γ (respectively, b and v in the $\hat{\mathbf{z}}$ direction), such that the absolute value of the acceleration in the $\hat{\mathbf{x}}$ direction is maximal.

By maximizing the acceleration, the noise is also maximized since the transfer function $S_{aa}(t) \propto a(t)^2$ and $\Gamma_n \propto S_{aa}(\omega) F(\omega)$, where the transfer function $F(\omega)$ is independent of the projection angles. Physically, it is clear that a larger acceleration causes a larger dephasing.

1. Charged interferometer

For a charged interferometer, the relevant angles that determine the movement of the external particle are α and β ; see Eq. (15). These angles are maximized to find an upper bound on the dephasing. Figures 7–9 show the acceleration

$$a(t) = \left| C \frac{\cos(\alpha) + (vt/b) \cos(\beta)}{[1 + (vt/b)^2]^a} \right| \quad (\text{B1})$$

as a function of the angles α and β . The magnitude of the acceleration is not given since it depends on the constant C , which is determined by the type of interaction (charged-charged, charged-permanent dipole, or charged-induced

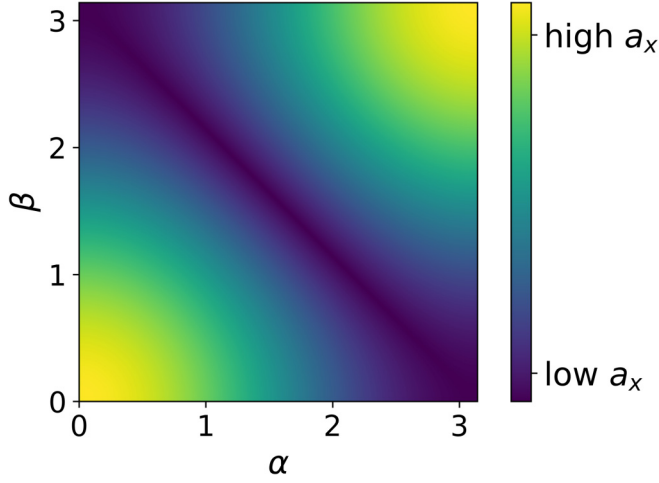


FIG. 8. For $vt/b = 1$ the absolute value of the acceleration [Eq. (B1) with $a = 3$] as a function of the projection angles $\alpha, \beta \in [0, \pi]$.

dipole). The value of a is also specified by the type of interaction, $a = 3/2, 2, 3$, see Eqs. (31), (33), (36).

The figures show that, for $vt > b$ by at least one order of magnitude, the acceleration is maximized for $\beta = 0, \pi$, and α arbitrarily. If $vt < b$ by at least one order of magnitude, then the plot rotates ninety degrees, and the maximum value of the acceleration is given by $\alpha = 0, \pi$, and β arbitrary. For $vt \sim b$ the maximization is given by $\alpha = \beta = 0$ or $\alpha = \beta = \pi$. Figures 7–9 are approximately constant for $a = 3/2, 2, 3$.

Therefore, a simple way to choose the angles such that the absolute acceleration from the interaction is maximized is to choose $\alpha = \beta = 0$ (or π).⁹

2. Neutral interferometer

For a neutral interferometer there are the additional angles γ and θ_0 that give the projection in the \hat{z} axis, see Eq. (A20).¹⁰ They are relevant because the interferometer dipole has been chosen to align with the \hat{z} axis.

Generically, we write the acceleration in the \hat{x} direction from the dipole-charge and dipole-dipole interactions as

$$a(t) = \left| C \frac{\cos(\alpha) + (vt/b) \cos(\beta)}{[1 + (vt/b)^2]^{5/2}} \times [\cos(\theta_0) + (vt/b) \cos(\gamma)] \right|, \quad (\text{B2})$$

with C a constant defined by the interaction. The angles α and θ_0 are related in the sense that if $\alpha = 0$, it means that $b = x_0$, and therefore $\theta_0 = \pi/2$ such that $b_z = 0$. Similarly the angles

⁹Note that, for the external dipole in Sec. IV, we assume that the particle has low velocity such that $|\mathbf{r} \cdot \mathbf{d}|(t) \approx |\mathbf{r} \cdot \mathbf{d}|$. So we have already made the assumptions on the magnitude of the velocity.

¹⁰Note that, for the induced dipole-charge interaction, these angles are not relevant, and the result for the projection angles for this interaction is the same as discussed in the previous section for the charged-interferometer case.

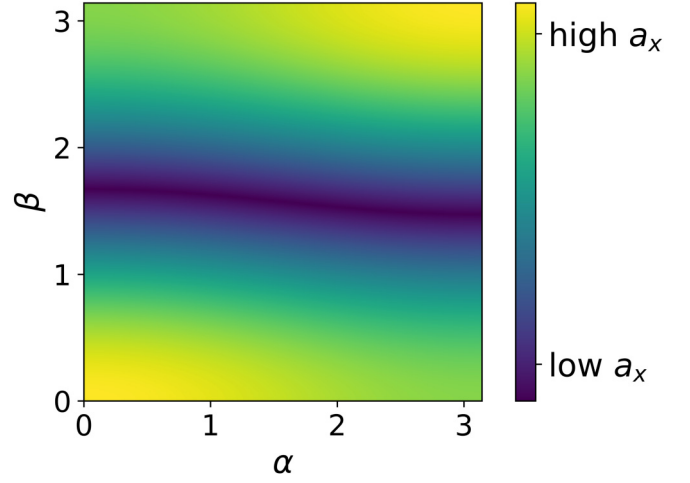


FIG. 9. For $vt/b = 10$ the absolute value of the acceleration [Eq. (B1) with $a = 3$] as a function of the projection angles $\alpha, \beta \in [0, \pi]$.

β and γ are related such that if $\beta = 0$, $v = v_x$ and thus $\gamma = \pi/2$, such that $v_z = 0$. Therefore, we define the dependency as

$$\cos(\theta_0) = \sqrt{1 - \cos^2(\alpha)}, \quad \cos(\gamma) = \sqrt{1 - \cos^2(\beta)}. \quad (\text{B3})$$

This follows from the Pythagorean theorem $v^2 = v_x^2 + v_y^2 + v_z^2$, where we have set $v_y = 0$ to maximize the acceleration.

The resulting plots that show the acceleration of Eq. (B2) as a function of α, β for arbitrary C are shown in Figs. 10–12. The figures are somewhat similar to Figs. 7–9, but one can see the extra dependence on the projection angles. From the figures, we can conclude that to maximize the acceleration generically, one can take the projection angles $\alpha = \beta = \pi/4, 3\pi/4$, which means that $\theta_0 = \gamma = \pi/4, 3\pi/4$.

In the case of a dipole-dipole interaction, the assumption that the particle has low velocity such that $\mathbf{r}(t) \cdot \mathbf{d}$ is approximately constant in time removes the dependence on γ .

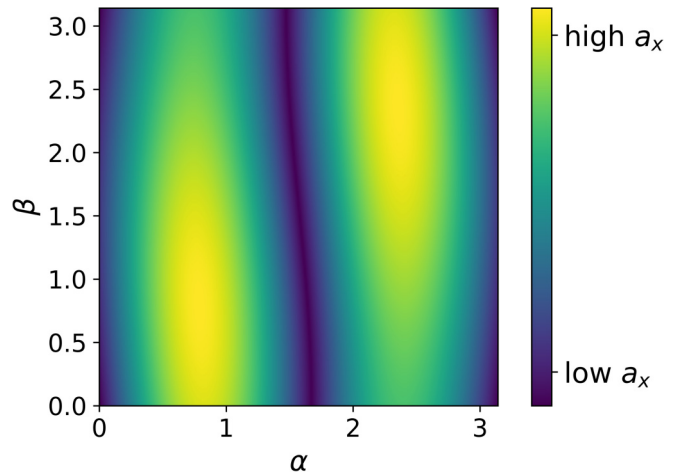


FIG. 10. For $vt/b = 0.1$ the absolute value of the acceleration [Eq. (B2)] as a function of the projection angles $\alpha, \beta \in [0, \pi]$.

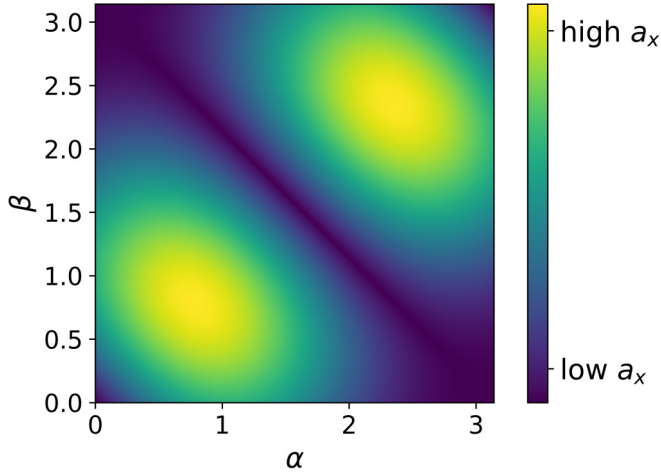


FIG. 11. For $vt/b = 1$ the absolute value of the acceleration [Eq. (B2)] as a function of the projection angles $\alpha, \beta \in [0, \pi]$.

The resulting plot looks very similar to Fig. 10 and shows that the acceleration is maximal for $\alpha = \pi/4, \beta = 0$ and for $\alpha = 3\pi/4, \beta = \pi$, see Fig. 13.

APPENDIX C: APPROXIMATIONS OF THE AVERAGED DEPHASING

In Sec. VII, the averaged acceleration noise PSD of Eq. (17) was used with the probability distributions over the impact parameter and projection angles (chosen to be a uniform distribution), and the velocity (determined to be a Maxwell-Boltzmann distribution). For small temperatures, the width of the Maxwell-Boltzmann distribution becomes small and has most probable velocity $\bar{v} = \sqrt{2k_b T_{\text{gas}}/m_{\text{gas}}}$. We, therefore, consider the Maxwell-Boltzmann distribution to be a Dirac-delta distribution at $v = \bar{v}$, which holds approximately for $T_{\text{gas}} \leq 0.1$ mK. Since there is an integration over v and b , taking $T = b/v$ as the characteristic timescale does not make sense anymore, and instead we take $T = 10\tau$ such that the timescale of the noise is larger than the interferometer time and thus Eq. (4) holds. To simplify the calculation, we make

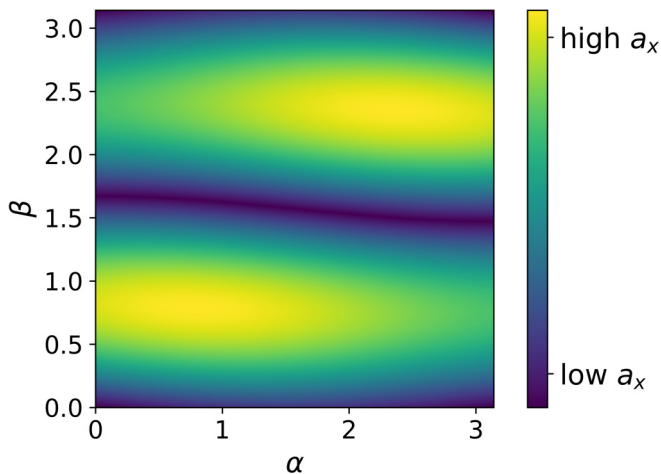


FIG. 12. For $vt/b = 10$ the absolute value of the acceleration [Eq. (B2)] as a function of the projection angles $\alpha, \beta \in [0, \pi]$.

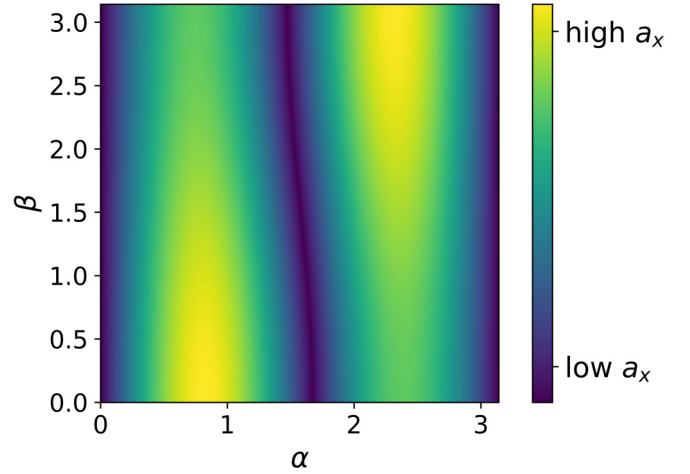


FIG. 13. For $vt/b = 0.1$ the absolute value of the acceleration for the dipole case [Eq. (B2) without the $\cos(\gamma)$ term] as a function of the projection angles $\alpha, \beta \in [0, \pi]$.

further assumptions such that the Bessel functions can be approximated. The modified Bessel functions of the second kind arise from the Fourier transform of the acceleration, see Appendix A and more concretely Eqs. (A25), (A28) for the relevant acceleration PSDs used in the QGEM case and Eq. (A11) for the PSD used in the CNOT case. These PSDs are used in this section in Eq. (17) to find the averaged acceleration noise PSD given the distributions in Eqs. (18)–(21). The Bessel functions that are contained in these PSDs can be approximated with the expansion in Eqs. (C3) and (C6), depending on the parameters of the experiment.

1. Approximations involved in the QGEM setup

We approximate the integration over ω to get the total dephasing by substituting the dominant mode $\omega = \omega_{\min}$. This can be understood physically as considering the dephasing at the longest experimental time. Mathematically, the transfer function [see Eq. (13)] shows strong decay for increasing ω , showing that the minimal value is dominant and that the approximation is applicable due to the fast decline. For $\omega = \omega_{\min} = 2\pi/\tau = 2\pi$ Hz, the argument of the Bessel function is [see Eqs. (45), (42), and (47)]

$$\frac{2\pi R}{\sqrt{2k_b T_{\text{gas}}/m_{\text{gas}}}} \leq \frac{b\omega_{\min}}{\bar{v}} \leq \frac{2\pi L}{\sqrt{2k_b T_{\text{gas}}/m_{\text{gas}}}}, \quad (\text{C1})$$

where m_{gas} denotes the mass of air molecules and we set $T_{\text{gas}} = 10^{-4}$ K. For these parameters we can also approximate the Maxwell-Boltzmann distribution as discussed in the main text. For a spherical diamond of mass 10^{-15} kg (i.e., a radius of ≈ 1 μm) and an experimental chamber of $L = 0.01$ m, which are parameters applicable to the QGEM experiment, the argument of the Bessel function is small in the limit which we are considering in our computation:

$$b\omega_{\min}/\bar{v} < 1 \quad \text{for } b \in [R, L]. \quad (\text{C2})$$

Therefore, we approximate the modified Bessel functions of the second kind as follows:

$$K_n(u) \approx \frac{\Gamma(n)}{2} \left(\frac{2}{u}\right)^n \text{ for } 0 < |u| \leq \sqrt{n+1} \text{ and } n > 0. \quad (\text{C3})$$

With the approximate Bessel function, we find the dephasing of the dominant mode presented in Fig. 5 as a function of the number density $n_v = N/V$ with $V = L^3$.

2. Approximations involved in the CNOT setup

For $\omega = \omega_{\min} = 2\pi/\tau = 2\pi \times 10^{-6}$ Hz, the argument of the Bessel function is given by

$$\frac{2\pi b_{\min}}{\sqrt{2k_b T_{\text{gas}}/m_{\text{gas}}}} \leq \frac{b\omega}{\bar{v}}, \quad (\text{C4})$$

where m_{gas} is the mass of air molecules, and $T_{\text{gas}} = 10^{-4}$ K such that the Maxwell-Boltzmann distribution can be approximated as discussed in the main text. We find that the argument of the Bessel function is large:

$$b\omega/\bar{v} > 1 \text{ for } b \in [10^3 R, L] \text{ and } \omega \in [\omega_{\min}, \infty], \quad (\text{C5})$$

where we recall $L = 0.01$ m. To proceed analytically, we assume the minimal distance $b_{\min} = 10^3 R \approx 10^{-7}$ m, such that the modified Bessel functions of the second kind can be approximated via:

$$K_n(u) \approx e^{-u} \left[\left(\frac{\pi}{2u}\right)^{1/2} + \dots \right] \text{ for } u \rightarrow \infty. \quad (\text{C6})$$

With the approximate Bessel function, we find the dephasing after integrating over ω . This was presented in Fig. 6 as a function of the number density $n_v = N/V$ with $V = L^3$.

-
- [1] L. De Broglie, Waves and quanta, *Nature (London)* **112**, 540 (1923).
- [2] G. P. Thomson and A. Reid, Diffraction of cathode rays by a thin film, *Nature (London)* **119**, 890 (1927).
- [3] C. Davisson and L. H. Germer, Diffraction of electrons by a crystal of nickel, *Phys. Rev.* **30**, 705 (1927).
- [4] C. J. Davisson and L. H. Germer, Reflection and refraction of electrons by a crystal of nickel, *Proc. Natl. Acad. Sci. USA* **14**, 619 (1928).
- [5] E. Schrödinger, Die gegenwärtige Situation in der Quantenmechanik, *Naturwissenschaften* **23**, 807 (1935).
- [6] R. Colella, A. W. Overhauser, and S. A. Werner, Observation of gravitationally induced quantum interference, *Phys. Rev. Lett.* **34**, 1472 (1975).
- [7] V. V. Nesvizhevsky, H. G. Börner, A. K. Petukhov, H. Abele, S. Baeßler, F. J. Rueß, T. Stöferle, A. Westphal, A. M. Gagarski, G. A. Petrov *et al.*, Quantum states of neutrons in the earth's gravitational field, *Nature (London)* **415**, 297 (2002).
- [8] J. B. Fixler, G. Foster, J. McGuirk, and M. Kasevich, Atom interferometer measurement of the newtonian constant of gravity, *Science* **315**, 74 (2007).
- [9] P. Asenbaum, C. Overstreet, T. Kovachy, D. D. Brown, J. M. Hogan, and M. A. Kasevich, Phase shift in an atom interferometer due to spacetime curvature across its wave function, *Phys. Rev. Lett.* **118**, 183602 (2017).
- [10] C. Overstreet, P. Asenbaum, J. Curti, M. Kim, and M. A. Kasevich, Observation of a gravitational Aharonov-Bohm effect, *Science* **375**, 226 (2022).
- [11] R. J. Marshman, A. Mazumdar, G. W. Morley, P. F. Barker, S. Hoekstra, and S. Bose, Mesoscopic interference for metric and curvature (MIMAC) & gravitational wave detection, *New J. Phys.* **22**, 083012 (2020).
- [12] E. Kilian, M. Toroš, F. F. Deppisch, R. Saakyan, and S. Bose, Requirements on quantum superpositions of macro-objects for sensing neutrinos, *Phys. Rev. Res.* **5**, 023012 (2023).
- [13] P. F. Barker, S. Bose, R. J. Marshman, and A. Mazumdar, Entanglement based tomography to probe new macroscopic forces, *Phys. Rev. D* **106**, L041901 (2022).
- [14] A. Einstein, B. Podolsky, and N. Rosen, Can quantum-mechanical description of physical reality be considered complete? *Phys. Rev.* **47**, 777 (1935).
- [15] J. S. Bell, On the Einstein Podolsky Rosen paradox, *Phys. Phys. Fiz.* **1**, 195 (1964).
- [16] R. Horodecki, P. Horodecki, M. Horodecki, and K. Horodecki, Quantum entanglement, *Rev. Mod. Phys.* **81**, 865 (2009).
- [17] S. Bose, A. Mazumdar, G. W. Morley, H. Ulbricht, M. Toroš, M. Paternostro, A. A. Geraci, P. Barker, M. S. Kim, and G. Milburn, Spin entanglement witness for quantum gravity, *Phys. Rev. Lett.* **119**, 240401 (2017).
- [18] https://www.youtube.com/watch?v=0Fv-0k13s_k, 2016, accessed July 22, 2024.
- [19] C. Marletto and V. Vedral, Gravitationally-induced entanglement between two massive particles is sufficient evidence of quantum effects in gravity, *Phys. Rev. Lett.* **119**, 240402 (2017).
- [20] C. H. Bennett, D. P. DiVincenzo, J. A. Smolin, and W. K. Wootters, Mixed state entanglement and quantum error correction, *Phys. Rev. A* **54**, 3824 (1996).
- [21] R. J. Marshman, A. Mazumdar, and S. Bose, Locality and entanglement in table-top testing of the quantum nature of linearized gravity, *Phys. Rev. A* **101**, 052110 (2020).
- [22] S. Bose, A. Mazumdar, M. Schut, and M. Toroš, Mechanism for the quantum natured gravitons to entangle masses, *Phys. Rev. D* **105**, 106028 (2022).
- [23] A. Sørensen and K. Mølmer, Quantum computation with ions in thermal motion, *Phys. Rev. Lett.* **82**, 1971 (1999).
- [24] D. Biswas, S. Bose, A. Mazumdar, and M. Toroš, Gravitational optomechanics: Photon-matter entanglement via graviton exchange, *Phys. Rev. D* **108**, 064023 (2023).
- [25] S. Bose, A. Mazumdar, M. Schut, and M. Toroš, Entanglement witness for the weak equivalence principle, *Entropy* **25**, 448 (2022).
- [26] S. Chakraborty, A. Mazumdar, and R. Pradhan, Distinguishing Jordan and Einstein frames in gravity through entanglement, *Phys. Rev. D* **108**, L121505 (2023).
- [27] S. G. Elahi and A. Mazumdar, Probing massless and massive gravitons via entanglement in a warped extra dimension, *Phys. Rev. D* **108**, 035018 (2023).

- [28] U. K. Beekering Vinckers, A. de la Cruz-Dombriz, and A. Mazumdar, Quantum entanglement of masses with non-local gravitational interaction, *Phys. Rev. D* **107**, 124036 (2023).
- [29] F. Hanif, D. Das, J. Halliwell, D. Home, A. Mazumdar, H. Ulbricht, and S. Bose, Testing whether gravity acts as a quantum entity when measured, [arXiv:2307.08133](https://arxiv.org/abs/2307.08133).
- [30] T. W. van de Kamp, R. J. Marshman, S. Bose, and A. Mazumdar, Quantum gravity witness via entanglement of masses: Casimir screening, *Phys. Rev. A* **102**, 062807 (2020).
- [31] M. Scala, M. S. Kim, G. W. Morley, P. F. Barker, and S. Bose, Matter-wave interferometry of a levitated thermal nanoscillator induced and probed by a spin, *Phys. Rev. Lett.* **111**, 180403 (2013).
- [32] C. Wan, M. Scala, G. W. Morley, A. T. M. A. Rahman, H. Ulbricht, J. Bateman, P. F. Barker, S. Bose, and M. S. Kim, Free nano-object Ramsey interferometry for large quantum superpositions, *Phys. Rev. Lett.* **117**, 143003 (2016).
- [33] Y. Margalit, O. Dobkowski, Z. Zhou, O. Amit, Y. Japha, S. Moukouri, D. Rohrllich, A. Mazumdar, S. Bose, C. Henkel, and R. Folman, Realization of a complete Stern-Gerlach interferometer: Towards a test of quantum gravity, *Sci. Adv.* **7**, eabg2879 (2021).
- [34] R. J. Marshman, A. Mazumdar, R. Folman, and S. Bose, Constructing nano-object quantum superpositions with a Stern-Gerlach interferometer, *Phys. Rev. Res.* **4**, 023087 (2022).
- [35] S. Machluf, Y. Japha, and R. Folman, Coherent Stern-Gerlach momentum splitting on an atom chip, *Nat. Commun.* **4**, 2424 (2013).
- [36] O. Amit, Y. Margalit, O. Dobkowski, Z. Zhou, Y. Japha, M. Zimmermann, M. A. Efremov, F. A. Narducci, E. M. Rasel, W. P. Schleich, and R. Folman, T^3 stern-gerlach matter-wave interferometer, *Phys. Rev. Lett.* **123**, 083601 (2019).
- [37] R. Zhou, R. J. Marshman, S. Bose, and A. Mazumdar, Catapulting towards massive and large spatial quantum superposition, *Phys. Rev. Res.* **4**, 043157 (2022).
- [38] R. Zhou, R. J. Marshman, S. Bose, and A. Mazumdar, Mass-independent scheme for enhancing spatial quantum superpositions, *Phys. Rev. A* **107**, 032212 (2023).
- [39] R. Zhou, R. J. Marshman, S. Bose, and A. Mazumdar, Gravitodiamagnetic forces for mass independent large spatial quantum superpositions, [arXiv:2211.08435](https://arxiv.org/abs/2211.08435).
- [40] R. J. Marshman, S. Bose, A. Geraci, and A. Mazumdar, Entanglement of magnetically levitated massive Schrödinger cat states by induced dipole interaction, *Phys. Rev. A* **109**, L030401 (2024).
- [41] M. Schut, J. Tilly, R. J. Marshman, S. Bose, and A. Mazumdar, Improving resilience of quantum-gravity-induced entanglement of masses to decoherence using three superpositions, *Phys. Rev. A* **105**, 032411 (2022).
- [42] J. Tilly, R. J. Marshman, A. Mazumdar, and S. Bose, Qudits for witnessing quantum-gravity-induced entanglement of masses under decoherence, *Phys. Rev. A* **104**, 052416 (2021).
- [43] J. S. Pedernales, G. W. Morley, and M. B. Plenio, Motional dynamical decoupling for interferometry with macroscopic particles, *Phys. Rev. Lett.* **125**, 023602 (2020).
- [44] S. Rijavec, M. Carlesso, A. Bassi, V. Vedral, and C. Marletto, Decoherence effects in non-classicality tests of gravity, *New J. Phys.* **23**, 043040 (2021).
- [45] O. Romero-Isart, A. C. Pflanzer, F. Blaser, R. Kaltenbaek, N. Kiesel, M. Aspelmeyer, and J. I. Cirac, Large quantum superpositions and interference of massive nanometer-sized objects, *Phys. Rev. Lett.* **107**, 020405 (2011).
- [46] D. E. Chang, C. A. Regal, S. B. Papp, D. J. Wilson, J. Ye, O. Painter, H. J. Kimble, and P. Zoller, Cavity opto-mechanics using an optically levitated nanosphere, *Proc. Natl. Acad. Sci. USA* **107**, 1005 (2010).
- [47] M. Schlosshauer, The quantum-to-classical transition and decoherence, [arXiv:1404.2635](https://arxiv.org/abs/1404.2635).
- [48] A. Bassi, K. Lochan, S. Satin, T. P. Singh, and H. Ulbricht, Models of wave-function collapse, underlying theories, and experimental tests, *Rev. Mod. Phys.* **85**, 471 (2013).
- [49] M. Toroš, A. Mazumdar, and S. Bose, Loss of coherence of matter-wave interferometer from fluctuating graviton bath, *Phys. Rev. D* **109**, 084050 (2024).
- [50] P. Fragolino, M. Schut, M. Toroš, S. Bose, and A. Mazumdar, Decoherence of a matter-wave interferometer due to dipole-dipole interactions, *Phys. Rev. A* **109**, 033301 (2024).
- [51] P. R. Saulson, Terrestrial gravitational noise on a gravitational wave antenna, *Phys. Rev. D* **30**, 732 (1984).
- [52] D. J. Griffiths and D. F. Schroeter, *Introduction to Quantum Mechanics*, 3rd ed. (Cambridge University Press, Cambridge, New York, 2018).
- [53] M. Schlosshauer, Quantum decoherence, *Phys. Rep.* **831**, 1 (2019).
- [54] P. Storey and C. Cohen-Tannoudji, The Feynman path integral approach to atomic interferometry: A tutorial, *J. Phys. II* **4**, 1999 (1994).
- [55] M. Toroš, T. W. van de Kamp, R. J. Marshman, M. S. Kim, A. Mazumdar, and S. Bose, Relative acceleration noise mitigation for nanocrystal matter-wave interferometry: Applications to entangling masses via quantum gravity, *Phys. Rev. Res.* **3**, 023178 (2021).
- [56] M.-Z. Wu, M. Toroš, S. Bose, and A. Mazumdar, Quantum gravitational sensor for space debris, *Phys. Rev. D* **107**, 104053 (2023).
- [57] M. Keil, S. Machluf, Y. Margalit, Z. Zhou, O. Amit, O. Dobkowski, Y. Japha, S. Moukouri, D. Rohrllich, Z. Binstock, Y. Bar-Haim, M. Givon, D. Groswasser, Y. Meir, and R. Folman, *Stern-Gerlach Interferometry with the Atom Chip* (Springer International Publishing, Cham, 2021), pp. 263–301.
- [58] C. Henkel, G. Jacob, F. Stopp, F. Schmidt-Kaler, M. Keil, Y. Japha, and R. Folman, Stern-Gerlach splitting of low-energy ion beams, *New J. Phys.* **21**, 083022 (2019).
- [59] M. G. Raizen, J. M. Gilligan, J. C. Bergquist, W. M. Itano, and D. J. Wineland, Ionic crystals in a linear Paul trap, *Phys. Rev. A* **45**, 6493 (1992).
- [60] C. Monroe, D. M. Meekhof, B. E. King, W. M. Itano, and D. J. Wineland, Demonstration of a fundamental quantum logic gate, *Phys. Rev. Lett.* **75**, 4714 (1995).
- [61] D. Kielpinski, A. Ben-Kish, J. Britton, V. Meyer, M. A. Rowe, C. A. Sackett, W. M. Itano, C. Monroe, and D. J. Wineland, Recent results in trapped-ion quantum computing, [arXiv:quant-ph/0102086](https://arxiv.org/abs/quant-ph/0102086).
- [62] B. D. Wood, S. Bose, and G. W. Morley, Spin dynamical decoupling for generating macroscopic superpositions of a free-falling nanodiamond, *Phys. Rev. A* **105**, 012824 (2022).

- [63] J. Schwinger, M. O. Scully, and B. G. Englert, Is spin coherence like Humpty-Dumpty? *Z. Phys. D: At. Mol. Clusters* **10**, 135 (1988).
- [64] M. O. Scully, B.-G. Englert, and J. Schwinger, Spin coherence and Humpty-Dumpty. III. The effects of observation, *Phys. Rev. A* **40**, 1775 (1989).
- [65] B. Englert, J. Schwinger, and M. O. Scully, Is spin coherence like Humpty-Dumpty? I. Simplified treatment, *Found. Phys.* **18**, 1045 (1988).
- [66] N. Wiener, Generalized harmonic analysis, *Acta Math.* **55**, 117 (1930).
- [67] A. Khintchine, Korrelationstheorie der stationären stochastischen Prozesse, *Math. Ann.* **109**, 604 (1934).
- [68] C. Chatfield, and H. Xing, *The Analysis of Time Series: An Introduction with R*, 6th ed., (Chapman and Hall/CRC, New York, 2019).
- [69] Y. Japha and R. Folman, Role of rotations in Stern-Gerlach interferometry with massive objects, *Phys. Rev. Lett.* **130**, 113602 (2023).
- [70] M. Frimmer, K. Luszcz, S. Ferreira, V. Jain, E. Hebestreit, and L. Novotny, Controlling the net charge on a nanoparticle optically levitated in vacuum, *Phys. Rev. A* **95**, 061801(R) (2017).
- [71] D. J. Griffiths, *Introduction to Electrodynamics* (Cambridge University Press, Cambridge, 2013).
- [72] J. D. Jackson, *Classical Electrodynamics*, 3rd ed. (Wiley, New York, 1999).
- [73] D. Lide, *CRC Handbook of Chemistry and Physics*, 85th ed. (Taylor & Francis, 2004).
- [74] <https://www.noaa.gov/jetstream/atmosphere>, accessed July 22, 2024.
- [75] <https://cccbdb.nist.gov/pollistx.asp>, accessed July 22, 2024.
- [76] G. Afek, F. Monteiro, B. Siegel, J. Wang, S. Dickson, J. Recoaro, M. Watts, and D. C. Moore, Control and measurement of electric dipole moments in levitated optomechanics, *Phys. Rev. A* **104**, 053512 (2021).
- [77] M. Schut, A. Geraci, S. Bose, and A. Mazumdar, Micron-size spatial superpositions for the QGEM-protocol via screening and trapping, *Phys. Rev. Res.* **6**, 013199 (2023).
- [78] H. Chevalier, A. J. Paige, and M. S. Kim, Witnessing the nonclassical nature of gravity in the presence of unknown interactions, *Phys. Rev. A* **102**, 022428 (2020).
- [79] M. Schut, A. Grinin, A. Dana, S. Bose, A. Geraci, and A. Mazumdar, Relaxation of experimental parameters in a quantum-gravity induced entanglement of masses protocol using electromagnetic screening, *Phys. Rev. Res.* **5**, 043170 (2023).
- [80] D. L. Danielson, G. Satishchandran, and R. M. Wald, Gravitationally mediated entanglement: Newtonian field versus gravitons, *Phys. Rev. D* **105**, 086001 (2022).
- [81] D. Carney, P. C. E. Stamp, and J. M. Taylor, Tabletop experiments for quantum gravity: A user's manual, *Class. Quant. Grav.* **36**, 034001 (2019).
- [82] D. Carney, Newton, entanglement, and the graviton, *Phys. Rev. D* **105**, 024029 (2022).
- [83] M. Christodoulou *et al.*, Locally mediated entanglement through gravity from first principles, *Phys. Rev. Lett.* **130**, 100202 (2022).
- [84] N. G. Van Kampen, *Stochastic Processes in Physics and Chemistry* (Elsevier, North-Holland, 1992), Vol. 1.
- [85] A. Ibarra, M. Gonzalez, R. Vila, and J. Molla, Wide frequency dielectric properties of CVD diamond, *Diam. Relat. Mater.* **6**, 856 (1997).
- [86] U. Delić, M. Reisenbauer, K. Dare, D. Grass, V. Vuletić, N. Kiesel, and M. Aspelmeyer, Cooling of a levitated nanoparticle to the motional quantum ground state, *Science* **367**, 892 (2020).